A Theory for the Design of Multi-Stable Morphing Structures

Yang Li, Sergio Pellegrino*

Graduate Aerospace Laboratories California Institute of Technology 1200 E. California Blvd, Pasadena, CA 91125, United States

ARTICLE INFO

ABSTRACT

Multi-stable structures can provide desired reconfigurability and require relatively simple actuation. This paper considers general bar and plate structures connected by frictionless hinges that are to be made locally stable in a set of chosen target configurations by attaching extensional and rotational, linear-elastic springs to the structure. The unstressed lengths and angles of the springs, as well as their stiffnesses, are the unknown design parameters to be determined. A set of equilibrium and stability conditions to be satisfied in each of the target configurations of the structure are derived. Solutions of these equations provide specific values of the spring properties that correspond to local energy minima in all of the target configurations. The formulation is fully general and is applicable to structures of any complexity. A simple example is used to illustrate the design process for a bi-stable origami structure and a physical prototype is also presented.

1. Introduction

Structures that operate in multiple configurations have wide-ranging applications. Examples include the control surfaces for the wings of aircraft (Arrieta et al., 2013; Daynes et al., 2010; Niu, 2011) and morphing air inlets (Daynes et al., 2011) that are required to change their geometric shapes to accommodate different operational requirements. Also, mechanical reconfiguration of reflector antennas is used to achieve beam steering and beam shaping (Clarricoats and Zhou, 1991; Washington, 1996). Variable geometry "morphing" structures can achieve multiple geometric configurations through an overall deformation process, without the addition of separate flaps, RF surfaces, mechanisms and actuators.

The literature on morphing structures, also called adaptive structures, is extensive. Adaptive structures for space infrastructure were the focus of many early studies (Chen and Wada, 1993; Miura et al., 1985; Rhodes and Mikulas, 1985) and a comprehensive review was published (Wada et al., 1990). More recent research has considered a broader range of applications, including vibration energy harvesting, vibration reduction, adaptive aeroelastic structures (Wagg et al., 2008).

The focus of the present paper is on applications that require structures with multiple, static operational configurations, which are called *target configurations*. In each of these configurations, the structure is locally stable and its stiffness is sufficient for the operation of the structure. The paper presents a general theory to design structures with local energy minima in the chosen target configurations, allowing the structures to be easily reconfigured between the target configurations with simple actuation. Kinematically determinate (Pellegrino and Calladine, 1986) rod-like truss structures consisting of bistable elements were studied in Schioler and Pellegrino (2007); they are an example of morphing structure that uses bistability at the component level. A constant force mechanism consisting of six curved beams (Venkiteswaran and Su, 2018) is an example of a planar structure optimized at the system level.

---

* Corresponding author.
E-mail address: sergiop@caltech.edu (S. Pellegrino).

Nomenclature

$\mathbf{A}$	$m \times m \times (n_b + n_r)$ third-order tensor of second-order extensions and rotations of the skeleton structure, due to unit amplitudes of all inextensional mechanisms
$\mathbf{A}_k^b$	$m \times m$ matrix of second-order extension of bar k, due to unit amplitudes of all inextensional mechanisms
$\mathbf{A}_r^h$	$m \times m$ matrix of second-order rotation of hinge r, due to unit amplitudes of all inextensional mechanisms
$\mathbf{B}^s$	$m \times m \times (p + q)$ third-order tensor of second-order spring extensions and rotations due to unit amplitudes of all inextensional mechanisms
$\mathbf{C}^b$	$n_b \times 3n$ compatibility matrix for all bars
$\mathbf{C}_k^b$	1×6 compatibility matrix for bar k
$\mathbf{C}^h$	$n_h \times 3n$ compatibility matrix for all hinges
$\mathbf{C}_r^h$	1×12 compatibility matrix for hinge r
$\mathbf{C}_k^{es}$	1×6 compatibility matrix for extensional spring k
$\mathbf{C}^s$	$(p + q) \times 3n$ compatibility matrix for all springs
$\mathbf{C}_r^{ts}$	1×12 compatibility matrix for torsional spring r
$\mathbf{d}, \mathbf{d}_c, \mathbf{d}_m, \mathbf{d}_n$	$3n$-component vectors of nodal displacements, correction displacements, first-order zero-energy displacements, second-order zero-energy displacements
$\mathbf{d}_i, \mathbf{d}_{ij}$	3-dimensional vector of displacements of node i, relative displacement of node j with respect to node i
$\mathbf{d}_k$	6-component vector of displacements for bar k
$\mathbf{d}_r$	12-component vector of displacement for hinge r
$\mathbf{e}$	n_b-dimensional vector of extensions of all bars
e_k	extension of bar k
$E_0, E_i, \Delta^1 E_i, \Delta^2 E_i$	strain energy in reference configuration, configuration i, first-order and second-order energy variations near configuration i
$\mathbf{H}_k^b$	6×6 Hessian matrix for bar k
$\mathbf{H}_k^{es}$	6×6 Hessian matrix for extensional spring k
$\mathbf{H}_r^h$	12×12 Hessian matrix for hinge r
$\mathbf{H}_r^{ts}$	12×12 Hessian matrix for torsional spring r
$\widetilde{\mathbf{H}}$	6×6 constant matrix
$\mathbf{K}$	$(p + q) \times (p + q)$ diagonal matrix with stiffnesses of all springs
m	number of inextensional mechanisms
$\mathbf{m}, \mathbf{n}$	normal vectors for hinge element
n, n_b, n_h, n_t	number of nodes, number of rigid bars, number of rigid hinges, number of target configurations
p	number of extensional springs
q	number of torsional springs
r_C	rank of compatibility matrix
$\mathbf{r}_{ij}$	3-dimensional vector along bar ij
$\mathbf{x}_i$	3-dimensional position vector for node i
$\mathbf{U}$	$(n_b + n_h) \times (n_b + n_h)$ matrix of left singular vectors
$\mathbf{U}_{r_C}$	$(n_b + n_h) \times r_C$ matrix of left singular vectors corresponding to non-zero singular values
$\mathbf{V}$	$(n_b + n_h) \times 3n$ matrix of singular values
$\mathbf{V}_{r_C}$	$r_C \times r_C$ diagonal matrix of non-zero singular values
$\mathbf{W}$	$3n \times 3n$ matrix of right singular vectors
$\mathbf{W}_c$	$m \times m \times 3n$ third-order tensor of second-order correction displacements due to unit amplitudes of all inextensional mechanisms
$\mathbf{W}_m$	$3n \times m$ matrix of first-order zero-energy displacements
$\mathbf{W}_{r_C}$	$3n \times r_C$ matrix of right singular vectors corresponding to non-zero singular values
$\boldsymbol{\alpha}^i$	m-dimensional vector of mechanisms' amplitudes for configuration i
β	acute inner angle of Miura-ori unit cell
$\boldsymbol{\theta}$	n_h-dimensional vector of rotations of all hinges
θ_r	rotation of hinge r
$\boldsymbol{\theta}^{ts}$	q-dimensional vector of rotations of all torsional springs
θ_r^{ts}	rotation of torsional spring r

Consider a kinematically indeterminate assembly of rigid bars and plates connected by frictionless pin-joints, with one or more zero-energy deformation modes (inextensional mechanisms) (Pellegrino and Calladine, 1986). It will be called the

skeleton of the morphing structure, and it is assumed that there exists a continuous deformation of the structure that connects all of the specified target configurations. This skeleton can be transformed into a multi-stable structure by means of linear-elastic torsional and/or translational springs attached to the skeleton. The general problem is to find an elastic strain energy for the structure which, for the restricted motion space allowed by the zero-energy mechanisms of the skeleton, creates an energy landscape with multiple local minima. The energy landscape is controlled by two parameters for each spring, the rest length/angle and the stiffness. This paper presents a general formulation to compute the spring parameters that provide a specific set of local energy minima.

Previous research has been done to create such structures by attaching prestressed linear springs to single-degree-of-freedom mechanisms, and extensive studies of bi-stable four-bar linkages have made. Intuitive designs based on symmetry and snap-through behavior were proposed in Jensen and Howell (2004). Based on the complete kinematics of the planar four-bar linkage, the strain energy was expressed analytically in terms of one kinematic variable and other design parameters. By taking derivatives with respect to the kinematic variable, the corresponding equilibrium and stability constraints were formed. Solutions of these highly nonlinear equations were found with a homotopy solver (Su and Mc Carthy, 2007), substituting different design parameters into the equations until the constraints were satisfied (Jensen et al., 1999). A genetic algorithm was also used (King et al., 2005). Su and Mc Carthy (2007) specified the target equilibrium configurations, although their stability could not be guaranteed. The stability of another one degree of freedom mechanism, a three-dimensional Miura-ori unit with linear springs attached, was demonstrated in Waitukaitis et al. (2015). Instead of formulating the constraint equations and solving them to find the spring parameters, random sampling of the design parameter space was employed to search for desired designs. This approach does not require analytical knowledge of the mechanism kinematics but becomes impractical for mechanisms with many degrees of freedom.

A method that allows specification of the target equilibrium configurations and only requires linearized kinematics has been proposed by the present authors (Li and Pellegrino, 2018) and a similar multi-equilibrium design method has been proposed in Stern et al. (2019). These latest studies can determine the spring design parameters that achieve specified equilibrium configurations, but without any guarantee regarding stability.

This paper is laid out as follows. Section 2 presents an introductory example for which designs with two stable configurations are obtained with a simple graphical construction. Section 3 formulates the general design problem. Section 4 presents the kinematic formulation to derive the first-order and second-order zero-energy mechanisms of the skeleton structure near the target configurations. Section 5 derives the equilibrium and stability conditions. A simple example that uses these conditions to design a bi-stable structure is presented in Section 6. Section 7 concludes the paper. A nomenclature list is also provided, followed by an Appendix with the matrices for the example in Section 6.

2. Introductory example

A simple bistable example will be used to introduce the proposed theory. Consider the four-bar linkage ABCD shown in Fig. 1, consisting of rigid bars of length $AB = 0.8$, $BC = 1.16$, $CD = 1.3$, and $AD = 0.95$. Two torsional springs of equal stiffness, k, are introduced at A and D. The relative rotations at A and D are denoted by θ_A and θ_D. These rotations are positive in the sense defined in the figure. Note that the chosen example skeleton has a single inextensional mechanism, i.e. there is only one way for it to move, in any given configuration. Also note that, by introducing only two elastic springs, we are setting up an example in which the strain energy function can be plotted as a two-dimensional contour plot. This will greatly aid the visualization of our results. Finally, note that there would be no difficulty to generalize the present example to springs of different stiffness and, indeed, use of different springs may be necessary to achieve some particular local energy minima.

It is assumed that the springs have rest angles, for which the spring moments are zero, respectively for $(\theta_A, \theta_D) = (\frac{3}{2}\pi, 3\pi)$, which have been chosen arbitrarily.

The strain energy of the linkage is given by:

$$E = \frac{1}{2}k\left(\theta_A - \frac{3}{2}\pi\right)^2 + \frac{1}{2}k(\theta_D - 3\pi)^2. \tag{1}$$

This quadratic function has a global minimum of exactly zero at $(\frac{3}{2}\pi, 3\pi)$, as shown in Fig. 2. However, this configuration, where the energy is a global minimum, is not kinematically admissible because a four-bar linkage has only one degree of freedom and hence there is only one value of θ_D compatible with any given value of θ_A. All kinematically admissible configurations for the structure are solutions of the equations (Mc Carthy and Soh, 2010):

$$\theta_D = \pi - \arctan\left(\frac{A_2}{A_1}\right) \pm \arccos\left(\frac{-A_3}{\sqrt{A_1^2 + A_2^2}}\right) \tag{2}$$

where

$$A_1 = 2AB \cdot CD \cos\theta_A - 2AD \cdot CD, \tag{3}$$
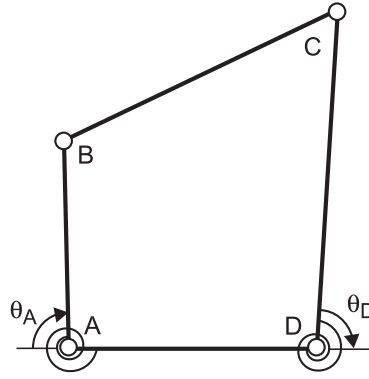
$$A_2 = 2AB \cdot CD \sin\theta_A, \tag{4}$$

Fig. 1. Four-bar linkage with two linear-elastic torsional springs.
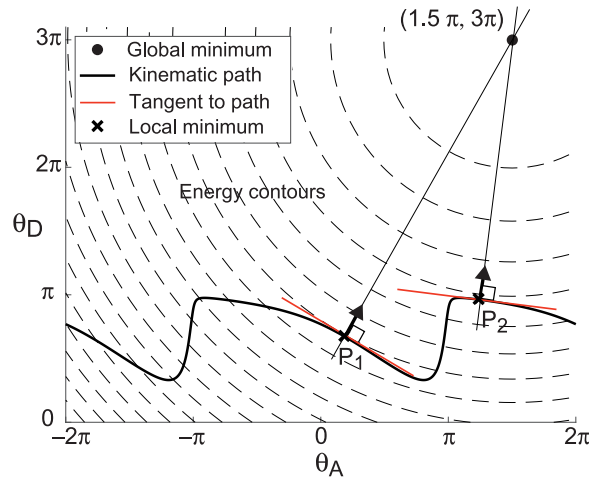

Fig. 2. Strain energy contours and kinematically admissible path of four-bar linkage of Fig. 1.

$$A_3 = AD^2 + CD^2 + AB^2 - BC^2 - 2AB \cdot AD \cos \theta_A. \tag{5}$$

This solution describes the kinematic path that has been plotted in Fig. 2 for the range $\theta_A = -2\pi, +2\pi$.

Coupling the kinematics of the four-bar linkage with the elastic strain energy in Eq. (1) excludes the global minimum of the energy. Therefore, instead of focusing on the global minimum of the energy, we search for local minima on the kinematically admissible path. The conditions for a kinematically admissible configuration to also be a local minimum of the energy are that (Thompson and Hunt, 1984):

Condition 1 The gradient of the energy should be orthogonal to the kinematic path for the energy to be locally stationary along the path.

Condition 2 The energy should locally increase on either side of this configuration for the stationary point to be a local minimum or, in other words, the kinematic path should lie on the opposite side of the tangent than the global energy minimum.

By drawing radial lines through the global energy minimum, it can be seen in Fig. 2 that there are only two configurations of the present linkage that satisfy these two conditions. These configurations correspond to the points P_1, P_2 marked with a black 'x' in Fig. 2, and which have angles $(\theta_A, \theta_D)^1 = (0.52, 2.15)$ and $(\theta_A, \theta_D)^2 = (3.87, 3.03)$. At this point it should be noted that by assigning arbitrary rest angles to the two springs we have obtained a bistable structure but the particular configurations in which the structure is bistable could not be chosen arbitrarily.

Next, consider the following design problem: to move the two local minima (black 'x' in Fig. 2) to general, specifically chosen configurations such as the points C_1 and C_2 marked by two red 'x' in Fig. 3, by finding suitable values for the spring rest angles. A possible approach, based on Waitukaitis et al. (2015), is to use an iterative scheme that searches for specific values of the spring parameters until the desired configurations of stable equilibrium are achieved. However, an alternative approach can be derived by focusing directly on Conditions 1 and 2.
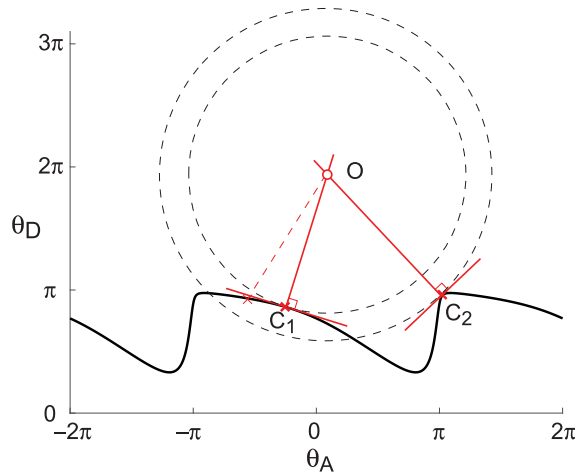
Fig. 3. Graphical solution of design problem with new global energy minimum at $(-0.08, 5.6)$.

Since the rest angles of the springs define the position of the energy minimum, a simple graphical solution can be obtained as follows. Let the two target configurations be $C_1 = (-0.80, 2.71)$ and $C_2 = (3.22, 3.02)$, as shown in Fig. 3. Consider the normal lines to the kinematic path through C_1 and C_2, shown in red. Consider a new global minimum for the energy, at the intersection $(-0.08, 5.6)$ of the two lines. This newly defined energy is stationary at C_1 and C_2 by construction, hence satisfying Condition 1. For the particular example considered here, it can also be verified that the kinematic path lies on the opposite side of the tangent from the energy minimum, for both C_1 and C_2, thus satisfying Condition 2.

If the kinematic path had curved towards the global energy minimum, with a curvature larger than the local curvature of the energy contour, the corresponding configuration would have been a local energy maximum, and hence the equilibrium would have been unstable. Satisfying Condition 2 requires the curvature of the energy contour to be compared with the curvature of the kinematic path.

For this example a simple graphical solution has been possible because there were only two unknown spring rest angles, and hence the whole design space could be analyzed by means of a two-dimensional plot. For more general problems, with larger numbers of degrees of freedom, springs, and target configurations, the obvious questions is how to find solutions in a higher-dimensional space. A general formulation that addresses this questions requires an extension of the ideas introduced in this section to the analysis of a convex (quadratic) energy combined with a non-convex kinematic manifold (Mc Carthy and Soh, 2010).

In summary, the design of multistable morphing structures consists in translating (changing the rest angles of the springs) and shaping (changing the stiffness of the springs) of a convex (quadratic) strain energy such that energy minima are achieved at specific points on the kinematic manifold. This requires considering simultaneously both first-order and second-order variations of the strain energy near each of the required configurations, within a fully general computational formulation.

3. Definition of design problem

Consider a bar and hinge structure consisting of a skeleton with n_b rigid bars and n_h rigid hinges, with p linear elastic extensional springs and q linear elastic torsional springs. Note that any three-dimensional bar-and-plate skeleton can be modeled in this way, by modeling the bars directly with pin-jointed bars, and subdividing the plates into triangles. Then, the edges of each triangle are modeled with pin-jointed bars and the planarity of the triangles that belong to the same plate is modeled by means of a no-rotation constraint (rigid hinge) along the common edges.

The number of unconstrained nodes of the structure is n and hence the total number of degrees of freedom is $3n$.

It is assumed that the structure is kinematically indeterminate (Pellegrino and Calladine, 1986), with m independent zero-energy mechanisms. n_t geometric configurations of the structure are defined and a kinematic simulation (not included in this paper) is carried out to verify that there is at least one continuous kinematic path connecting these n_t configurations. These are chosen as the *target configurations* of the structure, and it is desired that the structure is stable in each of these configurations. The target configurations of the structure are fully defined and, in particular, all nodal coordinates and hinge angles in each configuration are known.

For simplicity, it is assumed that the number of independent mechanisms is equal to m in all target configurations. This assumption excludes configurations of kinematic bifurcation (Kumar and Pellegrino, 2000), where the number of mechanisms may be locally larger, and also the possibility that, due to unilateral contacts, the number of mechanisms may be smaller in some target configurations.
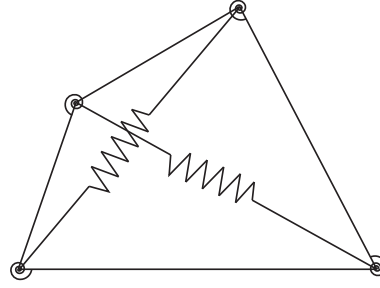
Fig. 4. Planar rigid four-bar linkage with 4 torsional and 2 translational springs.

Linear-elastic springs are added to the rigid bar-and-plate structure, transforming this "floppy" skeleton into an elastic structure. There are two types of springs: torsional springs at the hinges and extensional springs between pairs of nodes. An example consisting of 4 torsional and 2 extensional springs attached to a rigid four-bar linkage is shown in Fig. 4. For each spring, two design variables are introduced: the rest position (stress-free angle or length) and the stiffness.

For the structure to be in *stable equilibrium* in each of the n_t target configurations, it is required that all target configurations correspond to local minima of the total potential energy. No external loads will be considered, and hence the total potential energy is equal to the strain energy of the springs. Therefore, for any infinitesimally small perturbation along all kinematically admissible paths from all target configurations (Thompson and Hunt, 1984):

1. all first-order variations of the energy should be zero, and
2. all second-order variations of the energy should be positive.

Consider a general target configuration, i, with $i = (1, \ldots, n_t)$. A kinematic analysis of the structure is carried out in this configuration, to determine a full set of m independent, infinitesimal first-order mechanisms, with which an analysis of the equilibrium and stability of the structure near the target configuration can be carried out. Hence, a general first-order infinitesimal zero-energy deformation of the structure is defined by a linear combination of the m independent mechanisms in configuration i, where each mechanism is multiplied by the amplitude α_j^i with $j = (1, \ldots, m)$. The mechanism amplitudes are collected in the vector:

$$\boldsymbol{\alpha}^i = \begin{bmatrix} \alpha_1^i \\ \ldots \\ \alpha_j^i \\ \ldots \\ \alpha_m^i \end{bmatrix} \tag{6}$$

The variation of the total potential energy in the vicinity of configuration i is then analyzed for all possible mechanisms. The first derivatives of the energy with respect to the mechanisms' amplitudes are all set equal to zero. Hence, the above condition 1 is equivalent to m independent conditions for each configuration and therefore, for configuration i:

$$\left.\frac{\partial E}{\partial \alpha_1^i}\right|_{\text{config } i} = 0 \ldots, \quad \left.\frac{\partial E}{\partial \alpha_m^i}\right|_{\text{config } i} = 0 \quad \text{for } i = (1, \ldots, n_t) \tag{7}$$

These conditions were previously stated in Li and Pellegrino (2018) and Stern et al. (2019).

Regarding the positive definiteness of the second-order variations of the energy for target configuration i a quadratic form expresses the second-order variation of the energy for all possible mechanisms in configuration i:

$$(\boldsymbol{\alpha}^i)^{\text{T}} \begin{bmatrix} \left.\frac{\partial^2 E}{\partial(\alpha_1^i)^2}\right|_{\text{config } i} & \cdots & \left.\frac{\partial^2 E}{\partial\alpha_1^i\partial\alpha_m^i}\right|_{\text{config } i} \\ \vdots & \ddots & \vdots \\ \left.\frac{\partial^2 E}{\partial\alpha_m^i\partial\alpha_1^i}\right|_{\text{config } i} & \cdots & \left.\frac{\partial^2 E}{\partial(\alpha_m^i)^2}\right|_{\text{config } i} \end{bmatrix} \boldsymbol{\alpha}^i > 0 \quad \text{for } i = (1, \ldots, n_t) \tag{8}$$

This quadratic form has to be positive-definite in order to meet condition 2.

Eqs. (7) –(8) can be obtained directly if an analytical expression for the energy along the kinematically admissible path is available (Su and Mc Carthy, 2007), but this is only feasible for simple structures. In the next two sections Eqs. (7)–(8) will be obtained numerically for a general structure.

4. Kinematic analysis

As already mentioned in Section 3, the kinematic analysis detailed in this section is carried out for each target configuration, which can be reached through a continuous, purely kinematic motion of the bar-and-hinge skeleton structure.

4.1. Basic equations

Consider a general bar k of length L_k and connecting node i to node j. Taking the target configuration under study as the reference configuration, the position of node i is denoted by $\mathbf{x}_i$ with cartesian components x_i, y_i, z_i. The current position of node i, after imposing an infinitesimal deformation to the structure, is denoted by $\mathbf{x}_i + \mathbf{d}_i$ with cartesian components $x_i + u_i, y_i + v_i, z_i + w_i$.

The following vectors and notation are defined:

$$\mathbf{r}_{ji} = \mathbf{x}_j - \mathbf{x}_i = \begin{bmatrix} x_j - x_i \\ y_j - y_i \\ z_j - z_i \end{bmatrix} = \begin{bmatrix} x_{ji} \\ y_{ji} \\ z_{ji} \end{bmatrix} \tag{9}$$

and

$$\mathbf{d}_{ji} = \mathbf{d}_j - \mathbf{d}_i = \begin{bmatrix} u_j - u_i \\ v_j - v_i \\ w_j - w_i \end{bmatrix} = \begin{bmatrix} u_{ji} \\ v_{ji} \\ w_{ji} \end{bmatrix} \tag{10}$$

The extension of bar k, defined as its length in the infinitesimally deformed configuration minus the length in the target configuration (note that the extension is different from the Green-Lagrange strain derived in Kumar and Pellegrino (2000) and Liu and Paulino (2017)) is given by:

$$e_k = \|\mathbf{r}_{ji} + \mathbf{d}_{ji}\| - \|\mathbf{r}_{ji}\| \tag{11}$$

$$= \sqrt{(x_{ji} + u_{ji})^2 + (y_{ji} + v_{ji})^2 + (z_{ji} + w_{ji})^2} - \|\mathbf{r}_{ji}\| \tag{12}$$

$$= \sqrt{(x_{ji})^2 + 2x_{ji}u_{ji} + (u_{ji})^2 + \ldots} - \|\mathbf{r}_{ji}\| \tag{13}$$

$$= \left(\sqrt{1 + \frac{2x_{ji}u_{ji} + \ldots}{\|\mathbf{r}_{ji}\|^2} + \frac{(u_{ji})^2 + \ldots}{\|\mathbf{r}_{ji}\|^2}} - 1 \right) \|\mathbf{r}_{ji}\| \tag{14}$$

$$= \left(\sqrt{1 + \frac{2\mathbf{C}_k^b \mathbf{d}_k}{\|\mathbf{r}_{ji}\|} + \frac{(\mathbf{d}_k)^{\mathrm{T}} \widetilde{\mathbf{H}} \mathbf{d}_k}{\|\mathbf{r}_{ji}\|^2}} - 1 \right) \|\mathbf{r}_{ji}\| \tag{15}$$

where

$$\mathbf{C}_k^b = \begin{bmatrix} \frac{x_i - x_j}{L_k} & \frac{y_i - y_j}{L_k} & \frac{z_i - z_j}{L_k} & \frac{x_j - x_i}{L_k} & \frac{y_j - y_i}{L_k} & \frac{z_j - z_i}{L_k} \end{bmatrix} \tag{16}$$

is the compatibility matrix of the bar,

$$\widetilde{\mathbf{H}} = \begin{bmatrix} \mathbf{I}_{3\times3} & -\mathbf{I}_{3\times3} \\ -\mathbf{I}_{3\times3} & \mathbf{I}_{3\times3} \end{bmatrix} \tag{17}$$

and

$$\mathbf{d}_k = \begin{bmatrix} u_i \\ v_i \\ w_i \\ u_j \\ v_j \\ w_j \end{bmatrix} \tag{18}$$

The second and third terms inside the square root in Eq. (15) are infinitesimal quantities and hence the binomial expansion for the square root can be used. Including infinitesimal terms up to the second order, the expansion gives:

$$e_k \approx \left(1 + \frac{\mathbf{C}_k^b \mathbf{d}_k}{\|\mathbf{r}_{ji}\|} + \frac{(\mathbf{d}_k)^{\mathrm{T}} \widetilde{\mathbf{H}} \mathbf{d}_k}{2\|\mathbf{r}_{ji}\|^2} - \frac{(\mathbf{d}_k)^{\mathrm{T}} (\mathbf{C}_k^b)^{\mathrm{T}} \mathbf{C}_k^b \mathbf{d}_k}{2\|\mathbf{r}_{ji}\|^2} - 1 \right) \|\mathbf{r}_{ji}\| \tag{19}$$

simplifying this equation gives:

$$e_k \approx \mathbf{C}_k^b \mathbf{d}_k + \frac{(\mathbf{d}_k)^{\mathrm{T}} \widetilde{\mathbf{H}} \mathbf{d}_k}{2\|\mathbf{r}_{ji}\|} - \frac{(\mathbf{d}_k)^{\mathrm{T}} (\mathbf{C}_k^b)^{\mathrm{T}} \mathbf{C}_k^b \mathbf{d}_k}{2\|\mathbf{r}_{ji}\|} \tag{20}$$

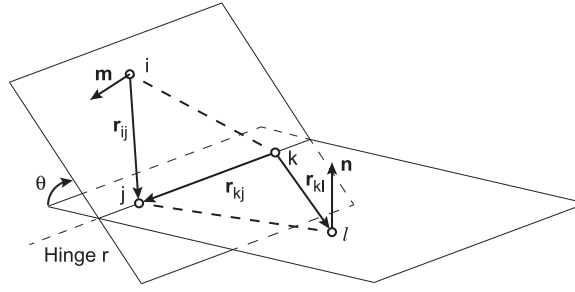where it should be noted that $\|\mathbf{r}_{ji}\| = L_k$.

Fig. 5. General hinge connection, based on Liu and Paulino (2017).

In conclusion, up to second-order infinitesimals, the extension induced by the displacement $\mathbf{d}_k$ of the nodes connected to bar k has the expression:

$$e_k = \mathbf{C}_k^b \mathbf{d}_k + \frac{1}{2L_k}(\mathbf{d}_k)^{\mathrm{T}} \mathbf{H}_k^b \mathbf{d}_k \tag{21}$$

where

$$\mathbf{H}_k^b = \widetilde{\mathbf{H}} - (\mathbf{C}_k^b)^{\mathrm{T}} \mathbf{C}_k^b \tag{22}$$

is the Hessian matrix for bar k.

Next, consider a general hinge connection, r, between the triangles connecting nodes i, j, k, l. The triangles may have been obtained by subdividing a square plate, in which case the triangles are initially coplanar and have to be constrained to remain coplanar. The general case of non-coplanar triangles connected by a hinge at an angle θ, as shown in Fig. 5, is considered here. $\theta = 0$ corresponds to coplanar triangles.

It has been shown in Liu and Paulino (2017) that, up to second-order infinitesimal quantities, the *hinge rotation* θ_r induced by the displacements $\mathbf{d}_r$ of nodes i, j, k, l is given by:

$$\theta_r = \mathbf{C}_r^h \mathbf{d}_r + \frac{1}{2} \mathbf{d}_r^{\mathrm{T}} \mathbf{H}_r^h \mathbf{d}_r, \tag{23}$$

where $\mathbf{C}_r^h$ is the 1×12 compatibility matrix for the hinge. Its components are given by

$$\frac{\partial \theta}{\partial \mathbf{x}_i} = -\frac{\|\mathbf{r}_{kj}\|}{\|\mathbf{m}\|^2} \mathbf{m}, \tag{24}$$

$$\frac{\partial \theta}{\partial \mathbf{x}_l} = \frac{\|\mathbf{r}_{kj}\|}{\|\mathbf{n}\|^2} \mathbf{n}, \tag{25}$$

$$\frac{\partial \theta}{\partial \mathbf{x}_j} = -\left(\frac{\mathbf{r}_{ij} \cdot \mathbf{r}_{kj}}{\|\mathbf{r}_{kj}\|^2} - 1 \right) \frac{\partial \theta}{\partial \mathbf{x}_i} + \frac{\mathbf{r}_{kl} \cdot \mathbf{r}_{kj}}{\|\mathbf{r}_{kj}\|^2} \frac{\partial \theta}{\partial \mathbf{x}_l}, \tag{26}$$

and

$$\frac{\partial \theta}{\partial \mathbf{x}_k} = -\left(\frac{\mathbf{r}_{kl} \cdot \mathbf{r}_{kj}}{\|\mathbf{r}_{kj}\|^2} - 1 \right) \frac{\partial \theta}{\partial \mathbf{x}_l} + \frac{\mathbf{r}_{ij} \cdot \mathbf{r}_{kj}}{\|\mathbf{r}_{kj}\|^2} \frac{\partial \theta}{\partial \mathbf{x}_i}, \tag{27}$$

where

$$\mathbf{r}_{pq} = \mathbf{x}_p - \mathbf{x}_q, \tag{28}$$

and the normal vectors $\mathbf{m}, \mathbf{n}$ are

$$\mathbf{m} = \mathbf{r}_{ij} \times \mathbf{r}_{kj} \quad \text{and} \quad \mathbf{n} = \mathbf{r}_{kj} \times \mathbf{r}_{kl}. \tag{29}$$

The matrix in the second term, $\mathbf{H}_r^h$, is the Hessian matrix for the hinge. It has size 12×12 and consists of 4×4 sub-matrices of size 3×3. This matrix is symmetric, and hence there are only 10 independent sub-matrices, which are provided in Appendix A of Liu and Paulino (2017) (Eqs. A (10) to A (20)). As an example, the 1,1 block is given by:

$$\frac{\partial^2 \theta}{\partial (\mathbf{x}_i)^2} = \frac{\|\mathbf{r}_{kj}\|}{\|\mathbf{m}\|^4} (\mathbf{m} \otimes (\mathbf{r}_{kj} \times \mathbf{m}) + (\mathbf{r}_{kj} \times \mathbf{m}) \otimes \mathbf{m}). \tag{30}$$

where $\otimes$ denotes a tensor product.

Note that in Liu and Paulino (2017) the initial angle between the triangles, θ, is defined as the dihedral angle of the triangle pair. This is different from the present definition and hence the signs of all entries in $\mathbf{C}_r^h$ and $\mathbf{H}_r^h$ provided in Liu and Paulino (2017) need to be swapped.

4.2. Zero-energy mechanisms

This section derives a general expression for the infinitesimal deformations of the skeleton structure that induce no extension of the bars and no distortion of the plates, up to second-order infinitesimal quantities.

The first-order equations of geometric compatibility for the structure are obtained by setting $e_k = 0$ in Eq. (21) and considering the first-order term only on the right-hand-side. Similarly, setting $\theta_r = 0$ in Eq. (23) and again considering the first-order term only on the right-hand-side. This gives $n_b + n_r$ equations in $3n$ unknown displacement components, $\mathbf{d}$. These first-order compatibility equations can be arranged in the form:

$$\begin{bmatrix} \mathbf{C}^b \\ \mathbf{C}^h \end{bmatrix} \mathbf{d} = \mathbf{0} \tag{31}$$

where $\mathbf{C}^b$, $\mathbf{C}^h$, are the compatibility matrices for the rigid bars and the rigid hinges, respectively.

The singular value decomposition (SVD) Strang (2006) of the compatibility matrix for the structure (Pellegrino, 1993) is then computed and it is given by:

$$\begin{bmatrix} \mathbf{C}^b \\ \mathbf{C}^h \end{bmatrix} = \mathbf{U}\mathbf{V}\mathbf{W}^{\mathrm{T}} \tag{32}$$

and the rank of the compatibility matrix is then given by the number of non-zero singular values, r_C. In general, the compatibility equations may not be independent, in which case:

$$r_C < n_b + n_h \tag{33}$$

The right-singular-vector matrix, $\mathbf{W}$, has size $3n \times 3n$. It is divided into two submatrices:

$$\mathbf{W} = [\mathbf{W}_{r_c} \mathbf{W}_m] \tag{34}$$

where the subscripts denote the number of columns of the submatrices.

The columns of $\mathbf{W}_m$ form an orthonormal set of zero-energy (to the first order) deformation modes for the structure. Therefore, a general zero-energy deformation mode has the expression

$$\mathbf{d}_m = \mathbf{W}_m \boldsymbol{\alpha}, \tag{35}$$

where $\boldsymbol{\alpha}$ contains m arbitrary coefficients.

The accuracy of the zero-energy deformation modes is increased to the second order by determining a correction, $\mathbf{d}_c$, for the displacement components. $\mathbf{d}_c$ is obtained by finding the second-order displacements that make the second-order bar extensions and hinge rotations equal to zero.

Determining this correction is easier if a *specific zero-energy mechanism* and hence a *specific vector* $\boldsymbol{\alpha}$ has been chosen. In this case, let this specific vector be $\overline{\boldsymbol{\alpha}}$. The specific first-order inextensional displacement is then

$$\overline{\mathbf{d}}_m = \mathbf{W}_m \overline{\boldsymbol{\alpha}} \tag{36}$$

The extension of bar k associated with the first-order inextensional displacement $\overline{\mathbf{d}}_m$ is obtained from Eq. (20), where the first term on the right-hand-side vanishes ($\mathbf{C}_k^b \mathbf{d}_k = 0$) because the displacement is first-order inextensional. The third term in Eq. (20) also vanishes ($(\mathbf{d}_k)^{\mathrm{T}}(\mathbf{C}_k^b)^{\mathrm{T}}\mathbf{C}_k^b \mathbf{d}_k = 0$) and therefore the Hessian matrix in Eq. (22) is simply:

$$\mathbf{H}_k^b = \widetilde{\mathbf{H}} \tag{37}$$

Then, substituting Eqs. (37) and (36) into Eq. (21) gives

$$\overline{e}_k = \frac{1}{2L_k} \overline{\boldsymbol{\alpha}}^{\mathrm{T}} (\mathbf{W}_m^{\mathrm{T}})_k \widetilde{\mathbf{H}} (\mathbf{W}_m)_k \overline{\boldsymbol{\alpha}} \tag{38}$$

where the subscript k denotes a submatrix of $\mathbf{W}_m$ containing only the 6 displacement components for the nodes of bar k. Defining the $m \times m$ matrix:

$$\mathbf{A}_k^b = \frac{1}{2L_k} (\mathbf{W}_m^{\mathrm{T}})_k \widetilde{\mathbf{H}} (\mathbf{W}_m)_k \tag{39}$$

Eq. (38) can be written as:

$$\overline{e}_k = \overline{\boldsymbol{\alpha}}^{\mathrm{T}} \mathbf{A}_k^b \overline{\boldsymbol{\alpha}} \tag{40}$$

Similarly, the second-order hinge rotations are obtained from Eq. (23). The first term on the right-hand-side vanishes because the nodal displacements are already first-order inextensional. Substituting Eq. (36) gives

$$\overline{\theta}_r = \frac{1}{2} \overline{\boldsymbol{\alpha}}^{\mathrm{T}} (\mathbf{W}_m^{\mathrm{T}})_r \mathbf{H}_r^h (\mathbf{W}_m)_r \overline{\boldsymbol{\alpha}} \tag{41}$$

where the subscript r denotes a submatrix of $\mathbf{W}_m$ containing only the 12 displacement components for the nodes of hinge r. Defining the $m \times m$ matrix:

$$\mathbf{A}_r^h = \frac{1}{2} (\mathbf{W}_m^{\mathrm{T}})_r \mathbf{H}_r^h (\mathbf{W}_m)_r \tag{42}$$

Eq. (41) can be written as:

$$\overline{\theta}_r = \overline{\boldsymbol{\alpha}}^{\mathrm{T}} \mathbf{A}_r^h \overline{\boldsymbol{\alpha}} \tag{43}$$

Collecting all of the second-order bar extensions and hinge rotations in a single column vector

$$\begin{bmatrix} \overline{\mathbf{e}} \\ \overline{\boldsymbol{\theta}} \end{bmatrix} = \begin{bmatrix} \vdots \\ \overline{e}_k \\ \vdots \\ \overline{\theta}_r \\ \vdots \end{bmatrix} = \begin{bmatrix} \vdots \\ \overline{\boldsymbol{\alpha}}^{\mathrm{T}} \mathbf{A}_k^b \overline{\boldsymbol{\alpha}} \\ \vdots \\ \overline{\boldsymbol{\alpha}}^{\mathrm{T}} \mathbf{A}_r^h \overline{\boldsymbol{\alpha}} \\ \vdots \end{bmatrix} \tag{44}$$

Then, the displacement correction for the first-order inextensional displacement in Eq. (36) can be computed by solving the compatibility equations

$$\begin{bmatrix} \mathbf{C}^b \\ \mathbf{C}^r \end{bmatrix} \overline{\mathbf{d}}_c = - \begin{bmatrix} \overline{\mathbf{e}} \\ \overline{\boldsymbol{\theta}} \end{bmatrix} \tag{45}$$

Using the SVD of the compatibility matrix, Eq. (32), and denoting by $(\mathbf{V}_{r_c})^{-1}$ the diagonal matrix with the reciprocals of the (non-zero) singular values, the solution orthogonal to the inextensional displacements is

$$\overline{\mathbf{d}}_c = -\mathbf{W}_{r_c} (\mathbf{V}_{r_c})^{-1} (\mathbf{U}_{r_c})^{\mathrm{T}} \begin{bmatrix} \overline{\mathbf{e}} \\ \overline{\boldsymbol{\theta}} \end{bmatrix} \tag{46}$$

and then, up to the second-order, the inextensional displacement is

$$\overline{\mathbf{d}} = \overline{\mathbf{d}}_m + \overline{\mathbf{d}}_c \tag{47}$$

This expression completes the solution for the case of a specific zero-energy displacement. In order to consider the case of a *general zero-energy displacement* the previous analysis can be repeated but, because no specific set of inextensional displacements has been chosen, the combined effects of all possible independent inextensional deformations have to be considered. Therefore, the calculation of the second-order bar extensions and hinge rotations has to account for all possible linear combinations of the independent mechanisms in the matrix $\mathbf{W}_m$.

As a first step, consider general amplitudes of an arbitrary pair (i, j) of independent mechanisms, corresponding to columns i and j of $\mathbf{W}_m$. This combined deformation mode can be obtained also from Eq. (36), for a specific choice of $\boldsymbol{\alpha}$:

$$\boldsymbol{\alpha}_{i,j} = \begin{bmatrix} 0 \\ \ldots \\ \alpha_i \neq 0 \\ 0 \\ \ldots \\ \alpha_j \neq 0 \\ 0 \\ \ldots \end{bmatrix} \tag{48}$$

Each entry in the vector of second-order bar extensions and hinge rotations for this particular combined mechanism is obtained by adding four quadratic terms:

$$\begin{bmatrix} \mathbf{e} \\ \boldsymbol{\theta} \end{bmatrix}_{i,j} = \begin{bmatrix} \vdots \\ \alpha_i (\mathbf{A}_k^b)_{i,i} \alpha_i + \alpha_i (\mathbf{A}_k^b)_{i,j} \alpha_j + \alpha_j (\mathbf{A}_k^b)_{j,i} \alpha_i + \alpha_j (\mathbf{A}_k^b)_{j,j} \alpha_j \\ \vdots \\ \alpha_i (\mathbf{A}_r^h)_{i,i} \alpha_i + \alpha_i (\mathbf{A}_r^h)_{i,j} \alpha_j + \alpha_j (\mathbf{A}_r^h)_{j,i} \alpha_i + \alpha_j (\mathbf{A}_r^h)_{j,j} \alpha_j \\ \vdots \end{bmatrix} \tag{49}$$

Hence, the displacement corrections for the first-order inextensional displacement

$$(\mathbf{d}_m)_{i,j} = \mathbf{W}_m \boldsymbol{\alpha}_{i,j} \tag{50}$$

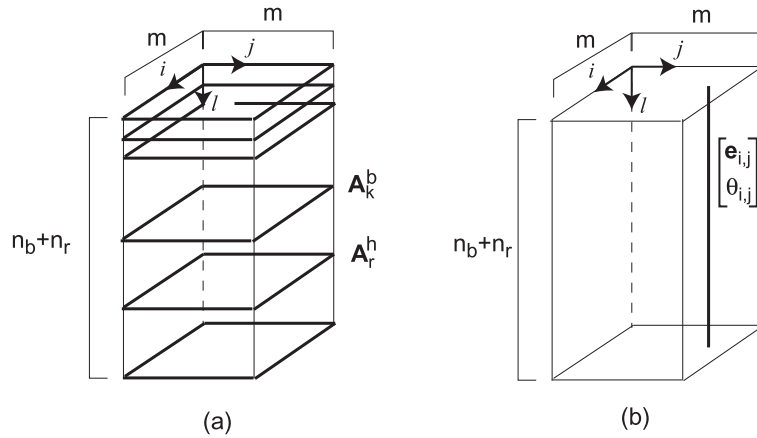**Fig. 6.** Two visualizations of the tensor **A** as (a) a stack of matrices and (b) a set of base vectors.

are calculated, in analogy with Eq. (46), from

$$(\mathbf{d}_c)_{i,j} = -\mathbf{W}_{r_c}(\mathbf{V}_{r_c})^{-1}(\mathbf{U}_{r_c})^{\mathrm{T}} \begin{bmatrix} \mathbf{e} \\ \boldsymbol{\theta} \end{bmatrix}_{i,j} \tag{51}$$

Finally, consider the fully general case where the independent mechanisms are multiplied by the general coefficients in the vector $\boldsymbol{\alpha}$ and hence the first-order inextensional displacement has the expression in Eq. (35). In this case, the second-order bar extensions and hinge rotations have to be expressed in terms of the general components of $\boldsymbol{\alpha}$. The resulting expression is a generalization of Eq. (49):

$$\begin{bmatrix} \mathbf{e} \\ \boldsymbol{\theta} \end{bmatrix} = \begin{bmatrix} \vdots \\ e_k \\ \vdots \\ \theta_r \\ \vdots \end{bmatrix} = \begin{bmatrix} \vdots \\ \sum_{i,j} \alpha_i (\mathbf{A}_k^b)_{i,j} \alpha_j \\ \vdots \\ \sum_{i,j} \alpha_i (\mathbf{A}_r^h)_{i,j} \alpha_j \\ \vdots \end{bmatrix} \tag{52}$$

where the summations are extended over the range $1 = 1, m$ and $j = 1, m$.

The following compact notation

$$\boldsymbol{\alpha}^{\mathrm{T}} \mathbf{A} \boldsymbol{\alpha} = \begin{bmatrix} \vdots \\ \sum_{i,j} \alpha_i (\mathbf{A}_k^b)_{i,j} \alpha_j \\ \vdots \\ \sum_{i,j} \alpha_i (\mathbf{A}_r^h)_{i,j} \alpha_j \\ \vdots \end{bmatrix} \tag{53}$$

is defined, and thus

$$\begin{bmatrix} \mathbf{e} \\ \boldsymbol{\theta} \end{bmatrix} = \boldsymbol{\alpha}^{\mathrm{T}} \mathbf{A} \boldsymbol{\alpha}, \tag{54}$$

where **A** is the $m \times m \times (n_b + n_r)$ third-order tensor consisting of the second-order extensions and rotations of the skeleton, due to unit amplitudes of all inextensional mechanisms, as shown in Fig. 6(a).

An equivalent expression is in terms of the base vectors

$$\begin{bmatrix} \mathbf{e}_{i,j} \\ \boldsymbol{\theta}_{i,j} \end{bmatrix} \tag{55}$$

that contain the second-order extensions and hinge rotations due to unit amplitudes of the mechanisms pair (i, j), as shown in Fig. 6(b). Then,

$$\begin{bmatrix} \mathbf{e} \\ \boldsymbol{\theta} \end{bmatrix} = \sum_{i,j} \begin{bmatrix} \mathbf{e}_{i,j} \\ \boldsymbol{\theta}_{i,j} \end{bmatrix} \alpha_i \alpha_j, \tag{56}$$

where

$$\begin{bmatrix} \mathbf{e}_{i,j} \\ \boldsymbol{\theta}_{i,j} \end{bmatrix} = \begin{bmatrix} \vdots \\ (\mathbf{A}_k^b)_{i,j} \\ \vdots \\ (\mathbf{A}_r^h)_{i,j} \\ \vdots \end{bmatrix}. \tag{57}$$

Lastly, the correction for the first-order displacements can be obtained by computing the displacements corresponding to each base vector. In analogy with Eq. (51), it is given by

$$(\mathbf{d}_c)_{i,j} = -\mathbf{W}_{r_c}(\mathbf{V}_{r_c})^{-1}(\mathbf{U}_{r_c})^{\mathrm{T}} \begin{bmatrix} \mathbf{e}_{i,j} \\ \boldsymbol{\theta}_{i,j} \end{bmatrix} \tag{58}$$

And then the complete set of correcting displacements is given by:

$$\mathbf{d}_c = \sum_{i,j} (\mathbf{d}_c)_{i,j} \alpha_i \alpha_j \tag{59}$$

The compact notation

$$\boldsymbol{\alpha}^{\mathrm{T}} \mathbf{W}_c \boldsymbol{\alpha} = \sum_{i,j} (\mathbf{d}_c)_{i,j} \alpha_i \alpha_j \tag{60}$$

is defined and hence

$$\mathbf{d}_c = \boldsymbol{\alpha}^{\mathrm{T}} \mathbf{W}_c \boldsymbol{\alpha} \tag{61}$$

where $\mathbf{W}_c$ is a rank 3 tensor with $m \times m \times 3n$ components.

In conclusion, the second-order compatible zero-energy deformation modes of the skeleton structure can be expressed as

$$\mathbf{d}_n = \mathbf{d}_m + \mathbf{d}_c = \mathbf{W_m}\boldsymbol{\alpha} + \boldsymbol{\alpha}^{\mathrm{T}} \mathbf{W_c} \boldsymbol{\alpha}. \tag{62}$$

4.3. Extensions and rotations of the springs

The elastic springs attached to the skeleton structure, as in the example shown in Fig. 4, undergo elastic deformation when a zero-energy deformation is imposed to the skeleton. The second-order spring extensions and rotations for a general second-order compatible deformation can be obtained by substituting the relevant nodal displacement components in $\mathbf{d}_n$ (Eq. (62)) in the corresponding compatibility equations (Eqs. (21) and (23)):

Consider a general translational spring k. Denoting by $(\mathbf{d}_n)_k$ the components of $\mathbf{d}_n$ that correspond to the nodes connected to spring k, Eq. (21) becomes

$$e_k = \mathbf{C}_k^{es}(\mathbf{d}_n)_k + \frac{1}{2L_k}(\mathbf{d}_n)_k^{\mathrm{T}} \mathbf{H}_k^{es}(\mathbf{d}_n)_k \tag{63}$$

where $\mathbf{C}_k^{es}$ and $\mathbf{H}_k^{es}$ (the superscript es denotes extensional springs) are the compatibility matrix and the Hessian matrix for an extensional spring.

Expanding $\mathbf{d}_n$ in Eq. (63) with Eq. (62) and neglecting terms higher than second order gives:

$$e_k = \mathbf{C}_k^{es}(\mathbf{W}_m)_k \boldsymbol{\alpha} + \mathbf{C}_k^{es}\left(\sum_{i,j}(\mathbf{d}_c)_{i,j}\alpha_i\alpha_j\right)_k + \boldsymbol{\alpha}^{\mathrm{T}}\frac{1}{2L_k}(\mathbf{W}_m)_k^{\mathrm{T}}\mathbf{H}_k^{es}(\mathbf{W}_m)_k\boldsymbol{\alpha} \tag{64}$$

The derivation can be repeated for a general torsional spring r to obtain:

$$\theta_r = \mathbf{C}_r^{ts}(\mathbf{W}_m)_r \boldsymbol{\alpha} + \mathbf{C}_r^{ts}\left(\sum_{i,j}(\mathbf{d}_c)_{i,j}\alpha_i\alpha_j\right)_r + \boldsymbol{\alpha}^{\mathrm{T}}\frac{1}{2}(\mathbf{W}_m)_r^{\mathrm{T}}\mathbf{H}_r^{ts}(\mathbf{W}_m)_r\boldsymbol{\alpha} \tag{65}$$

where $\mathbf{C}_r^{ts}$ and $\mathbf{H}_r^{ts}$ (the superscript ts denotes torsional springs) are the compatibility matrix and the Hessian matrix for a torsional spring.

Considering all extensional and rotational springs yields:

$$\begin{bmatrix} \mathbf{e} \\ \boldsymbol{\theta} \end{bmatrix}^s = \mathbf{C}^s \mathbf{W}_m \boldsymbol{\alpha} + \boldsymbol{\alpha}^{\mathrm{T}} \mathbf{B}^s \boldsymbol{\alpha} \tag{66}$$

where

$$\mathbf{C}^s \mathbf{W}_m = \begin{bmatrix} \vdots \\ \mathbf{C}_k^{es} (\mathbf{W}_m)_k \\ \vdots \\ \mathbf{C}_r^{ts} (\mathbf{W}_m)_r \\ \vdots \end{bmatrix} \tag{67}$$

and

$$\boldsymbol{\alpha}^{\mathrm{T}} \mathbf{B}^s \boldsymbol{\alpha} = \begin{bmatrix} \vdots \\ \mathbf{C}_k^{es} \left(\sum_{i,j} (\mathbf{d}_c)_{i,j} \alpha_i \alpha_j \right)_k + \boldsymbol{\alpha}^{\mathrm{T}} \frac{1}{2L_k} (\mathbf{W}_m)_k^{\mathrm{T}} \mathbf{H}_k^{es} (\mathbf{W}_m)_k \boldsymbol{\alpha} \\ \vdots \\ \mathbf{C}_r^{ts} \left(\sum_{i,j} (\mathbf{d}_c)_{i,j} \alpha_i \alpha_j \right)_r + \boldsymbol{\alpha}^{\mathrm{T}} \frac{1}{2} (\mathbf{W}_m)_r^{\mathrm{T}} \mathbf{H}_r^{ts} (\mathbf{W}_m)_r \boldsymbol{\alpha} \\ \vdots \end{bmatrix} \tag{68}$$

Here $\mathbf{B}^s$ is a rank 3 tensor with $m \times m \times (p+q)$ components. For any given configuration of the skeleton structure, all components of $\mathbf{B}^s$ are known.

5. Conditions for energy minima

In the initial, reference configuration of the structure (denoted by the subscript 0) the springs have initial extensions and rotations:

$$\begin{bmatrix} \mathbf{e} \\ \boldsymbol{\theta} \end{bmatrix}_0^s \tag{69}$$

which set up a state of prestress in the structure. Note that the sign of the *initial* extensions/rotations is opposite to the sign of the *rest* lengths/angles considered in Section 2. For example, a spring whose rest length is 1 mm too long has an initial extension of −1 mm in the reference configuration.

Defining the diagonal matrix $\mathbf{K}$ with the elastic spring stiffnesses along the main diagonal, the strain energy in the reference configuration has the expression:

$$E_0 = \frac{1}{2} \left(\begin{bmatrix} \mathbf{e}^{\mathrm{T}} & \boldsymbol{\theta}^{\mathrm{T}} \end{bmatrix}_0^s \right) \mathbf{K} \begin{bmatrix} \mathbf{e} \\ \boldsymbol{\theta} \end{bmatrix}_0^s \tag{70}$$

The structure is required to have local energy minima in n_t specified target configurations. The changes in spring extensions and rotations from the reference configuration to a general target configuration i, which can be obtained from a kinematic simulation of the type described in Kumar and Pellegrino (2000), are denoted by

$$\begin{bmatrix} \mathbf{e} \\ \boldsymbol{\theta} \end{bmatrix}_i^s \tag{71}$$

Consider the target configuration i. The strain energy is:

$$E_i = \frac{1}{2} \left(\begin{bmatrix} \mathbf{e}^{\mathrm{T}} & \boldsymbol{\theta}^{\mathrm{T}} \end{bmatrix}_i^s + \begin{bmatrix} \mathbf{e}^{\mathrm{T}} & \boldsymbol{\theta}^{\mathrm{T}} \end{bmatrix}_0^s \right) \mathbf{K} \left(\begin{bmatrix} \mathbf{e} \\ \boldsymbol{\theta} \end{bmatrix}_i^s + \begin{bmatrix} \mathbf{e} \\ \boldsymbol{\theta} \end{bmatrix}_0^s \right) \tag{72}$$

Next, compute the independent infinitesimal zero-energy deformation modes in configuration i and the corresponding extensions and rotations for the elastic springs. They have the general expression given by Eq. (66).

The strain energy near this configuration of the structure for general inextensional deformations of the skeleton is obtained by multiplying the current forces and moments by the extensions and rotations given by Eq. (66), and adding the change in the springs' strain energy due to these extensions and rotations. Therefore, the energy expression is:

$$E = E_i + \left(\begin{bmatrix} \mathbf{e}^{\mathrm{T}} & \boldsymbol{\theta}^{\mathrm{T}} \end{bmatrix}_i^s + \begin{bmatrix} \mathbf{e}^{\mathrm{T}} & \boldsymbol{\theta}^{\mathrm{T}} \end{bmatrix}_0^s \right) \mathbf{K} \left(\mathbf{C}^s|_i \mathbf{W}_m|_i \boldsymbol{\alpha}^i + (\boldsymbol{\alpha}^i)^{\mathrm{T}} \mathbf{B}^s|_i \boldsymbol{\alpha}^i \right) + \frac{1}{2} (\boldsymbol{\alpha}^i)^{\mathrm{T}} (\mathbf{W}_m|_i)^{\mathrm{T}} (\mathbf{C}^s|_i)^{\mathrm{T}} \mathbf{K} \mathbf{C}^s|_i \mathbf{W}_m|_i \boldsymbol{\alpha}^i \tag{73}$$

and the energy change can be expanded into infinitesimal terms of different order.

The first-order infinitesimal change is:

$$\Delta^1 E_i = \left(\begin{bmatrix} \mathbf{e}^{\mathrm{T}} & \boldsymbol{\theta}^{\mathrm{T}} \end{bmatrix}_i^s + \begin{bmatrix} \mathbf{e}^{\mathrm{T}} & \boldsymbol{\theta}^{\mathrm{T}} \end{bmatrix}_0^s \right) \mathbf{K} \, \mathbf{C}^s|_i \mathbf{W}_m|_i \boldsymbol{\alpha}^i \tag{74}$$

(a) Miura-ori unit cell.

(b) Simplified and labeled.

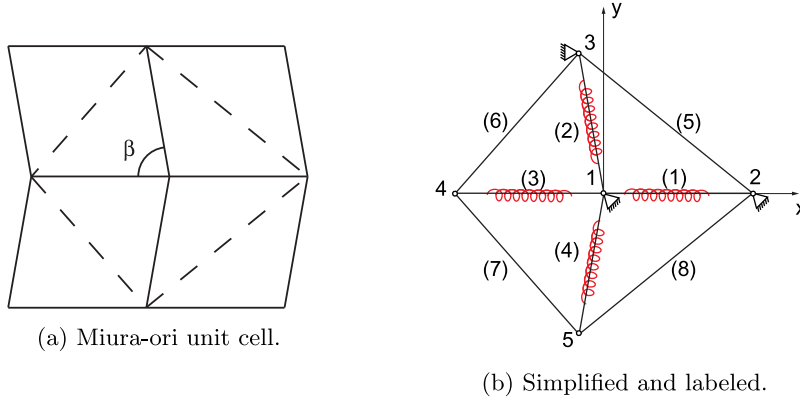**Fig. 7.** Reference configuration of Miura-ori unit cell.

The second-order infinitesimal change is:

$$\Delta^2 E_i = \left(\begin{bmatrix}\mathbf{e}^{\mathrm{T}} & \boldsymbol{\theta}^{\mathrm{T}}\end{bmatrix}_i^s + \begin{bmatrix}\mathbf{e}^{\mathrm{T}} & \boldsymbol{\theta}^{\mathrm{T}}\end{bmatrix}_0^s\right)\mathbf{K}\,(\boldsymbol{\alpha}^i)^{\mathrm{T}}\mathbf{B}|_i\boldsymbol{\alpha}^i + \frac{1}{2}(\boldsymbol{\alpha}^i)^{\mathrm{T}}(\mathbf{W}_m|_i)^{\mathrm{T}}(\mathbf{C}^s|_i)^{\mathrm{T}}\mathbf{K}\mathbf{C}^s|_i\mathbf{W}_m|_i\boldsymbol{\alpha}^i \tag{75}$$

Comparing Eq. (74) to Eq. (7), the equilibrium equations for configuration i are:

$$\left(\begin{bmatrix}\mathbf{e}^{\mathrm{T}} & \boldsymbol{\theta}^{\mathrm{T}}\end{bmatrix}_i^s + \begin{bmatrix}\mathbf{e}^{\mathrm{T}} & \boldsymbol{\theta}^{\mathrm{T}}\end{bmatrix}_0^s\right)\mathbf{K}\,\mathbf{C}^s|_i\mathbf{W}_m|_i = \mathbf{0} \tag{76}$$

and, comparing Eq. (75) to Eq. (8), the condition for the stability of configuration i is:

$$\left(\begin{bmatrix}\mathbf{e}^{\mathrm{T}} & \boldsymbol{\theta}^{\mathrm{T}}\end{bmatrix}_i^s + \begin{bmatrix}\mathbf{e}^{\mathrm{T}} & \boldsymbol{\theta}^{\mathrm{T}}\end{bmatrix}_0^s\right)\mathbf{K}\,(\boldsymbol{\alpha}^i)^{\mathrm{T}}\mathbf{B}|_i\boldsymbol{\alpha}^i + \frac{1}{2}(\boldsymbol{\alpha}^i)^{\mathrm{T}}(\mathbf{W}_m|_i)^{\mathrm{T}}(\mathbf{C}^s|_i)^{\mathrm{T}}\mathbf{K}\mathbf{C}_s|_i\mathbf{W}_m|_i\boldsymbol{\alpha}^i > 0 \tag{77}$$

This quadratic form has to be positive definite. This condition imposes m inequality constraints on the spring variables (stiffnesses and/or initial extensions or angles), for each target configuration.

For the structure to have an energy minimum in n_t target configurations there are $n_t \times m$ equality constraints (equilibrium) in addition to $n_t \times m$ inequalities (stability constraints) to be satisfied. Constrained optimization techniques can be employed to determine suitable designs of the springs.

6. An example

The application of the theory is demonstrated for the design of a simple bi-stable structure based on the Miura-ori folding pattern for a flat sheet (Miura, 1970). Miura-ori is an origami pattern widely used in engineering and has been studied extensively (Schenk and Guest, 2013).

The design of a Miura-ori unit cell with two stable configurations using four torsional springs of equal stiffness is considered. Since the hinge stiffness matrix $\mathbf{K} = \mathbf{I}$, the only design variables are the four initial rotations of the torsional springs.

All computations were carried out with Matlab (2018) and the main results are presented here to highlight the key steps of the analysis. See the section Research Data for details on the Matlab codes to carry out the computations.

6.1. Reference configuration

The Miura-ori unit cell flat configuration, chosen as the reference configuration, is shown in Fig. 7a. A simplified structure is shown and labeled in Fig. 7b. The numbering of nodes and bars is defined in the figure. Note that the outer triangles of the cell have been removed, for simplicity, and hence the rigid hinges that would be needed to hold the quadrilaterals planar in the original unit cell have also been removed. The inner acute angle of the unit cell is $\beta = 80°$ and the coordinates of the nodes in the reference configuration are:

$$\begin{bmatrix}\mathbf{x}_1 \\ \mathbf{x}_2 \\ \mathbf{x}_3 \\ \mathbf{x}_4 \\ \mathbf{x}_5\end{bmatrix}_0 = \begin{bmatrix} 0 & 0 & 0 \\ 1.0000 & 0 & 0 \\ -0.1736 & 0.9848 & 0 \\ -1.0000 & 0.0000 & 0 \\ -0.1736 & -0.9848 & 0 \end{bmatrix}, \tag{78}$$

Note that nodes 1, 2, and 3 are pinned to the ground. The displacement components of these constrained nodes are not included in the analysis.
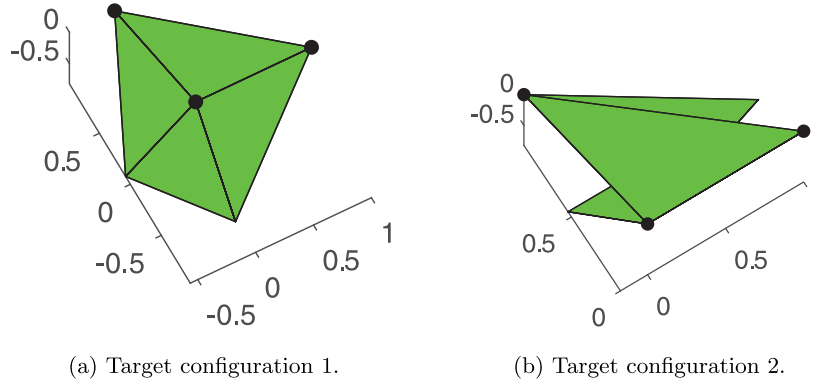
(a) Target configuration 1.   (b) Target configuration 2.

Fig. 8. Two target configurations.

The connections of the nodes by means of rigid bars and the bar lengths are respectively:

$$
\begin{bmatrix}
1 & 2 \\
1 & 3 \\
1 & 4 \\
1 & 5 \\
2 & 3 \\
3 & 4 \\
4 & 5 \\
5 & 2
\end{bmatrix}
\quad \text{and} \quad
\begin{bmatrix}
1.0000 \\
1.0000 \\
1.0000 \\
1.0000 \\
1.5321 \\
1.2856 \\
1.2856 \\
1.5321
\end{bmatrix}
\tag{79}
$$

However bars 1, 2 and 5 are not included in the analysis because both end nodes are constrained.

The initial angles of the four torsional springs, θ_0^s, are the four design variables to be determined.

6.2. Target configurations

Two target configurations are chosen, $n_t = 2$. Configuration 1 is shallowly folded and configuration 2 is deeply folded as shown in Fig. 8, where black dots indicate pinned foundations. The nodal coordinates of the two configurations are respectively:

$$
\begin{bmatrix}
\mathbf{x}_1 \\
\mathbf{x}_2 \\
\mathbf{x}_3 \\
\mathbf{x}_4 \\
\mathbf{x}_5
\end{bmatrix}_1
=
\begin{bmatrix}
0 & 0 & 0 \\
1.0000 & 0 & 0 \\
-0.1736 & 0.9848 & 0 \\
-0.5645 & 0.0768 & -0.8219 \\
-0.1736 & -0.9678 & -0.1824
\end{bmatrix}
\tag{80}
$$

and

$$
\begin{bmatrix}
\mathbf{x}_1 \\
\mathbf{x}_2 \\
\mathbf{x}_3 \\
\mathbf{x}_4 \\
\mathbf{x}_5
\end{bmatrix}_2
=
\begin{bmatrix}
0 & 0 & 0 \\
1.0000 & 0 & 0 \\
-0.1736 & 0.9848 & 0 \\
0.9226 & 0.3390 & -0.1843 \\
-0.1736 & 0.5354 & -0.8265
\end{bmatrix}.
\tag{81}
$$

The hinge rotations between the target configurations and the reference configuration are respectively:

$$
\theta_1^s =
\begin{bmatrix}
-0.1863 \\
-0.9873 \\
0.1863 \\
-0.9873
\end{bmatrix} \text{rad}
\quad \text{and} \quad
\theta_2^s =
\begin{bmatrix}
-2.1456 \\
-2.9533 \\
2.1456 \\
-2.9533
\end{bmatrix} \text{rad}.
\tag{82}
$$

6.3. Kinematic analysis

Since there are no rigid hinges in the skeleton structure, the compatibility matrix consists of $\mathbf{C}^b$ only. This matrix is computed in the target configurations to obtain:

$$\mathbf{C}^b|_1 = \begin{bmatrix} -0.5645 & 0.0768 & -0.8219 & 0 & 0 & 0 \\ 0 & 0 & 0 & -0.1736 & -0.9678 & -0.1824 \\ -0.3040 & -0.7063 & -0.6393 & 0 & 0 & 0 \\ -0.3040 & 0.8125 & -0.4974 & 0.3040 & -0.8125 & 0.4974 \\ 0 & 0 & 0 & -0.7660 & -0.6317 & -0.1191 \end{bmatrix}, \tag{83}$$

$$\mathbf{C}^b|_2 = \begin{bmatrix} 0.9226 & 0.3390 & -0.1843 & 0 & 0 & 0 \\ 0 & 0 & 0 & -0.1736 & 0.5354 & -0.8265 \\ 0.8527 & -0.5024 & -0.1434 & 0 & 0 & 0 \\ 0.8527 & -0.1528 & 0.4996 & -0.8527 & 0.1528 & -0.4996 \\ 0 & 0 & 0 & -0.7660 & 0.3495 & -0.5395 \end{bmatrix}. \tag{84}$$

The SVD's of $\mathbf{C}_b|_1$ and $\mathbf{C}_b|_2$ are then computed and the following $\mathbf{W}$ matrices are obtained:

$$\mathbf{W}|_1 = \begin{bmatrix} \mathbf{W}_{r_c} & \mathbf{W}_m \end{bmatrix}_1$$
$$= \begin{bmatrix} -0.2627 & 0.4192 & -0.0815 & -0.1964 & 0.2575 & -0.8023 \\ 0.3854 & 0.2208 & -0.6859 & 0.5052 & -0.2386 & -0.1415 \\ -0.4141 & 0.6995 & -0.1905 & -0.1128 & -0.0316 & 0.5379 \\ -0.0406 & -0.3046 & -0.5575 & -0.7215 & -0.2724 & 0.0000 \\ -0.7622 & -0.4231 & -0.2584 & 0.4137 & 0.0198 & -0.0401 \\ 0.1683 & -0.1204 & -0.3301 & -0.0416 & 0.8951 & 0.2130 \end{bmatrix} \tag{85}$$

and

$$\mathbf{W}|_2 = \begin{bmatrix} \mathbf{W}_{r_c} & \mathbf{W}_m \end{bmatrix}_2$$
$$= \begin{bmatrix} 0.6265 & -0.7549 & -0.1595 & 0.0601 & -0.0838 & -0.0401 \\ -0.0926 & 0.0727 & -0.3026 & 0.9412 & -0.0927 & -0.0071 \\ 0.1491 & 0.1188 & 0.5299 & 0.0963 & -0.7924 & -0.2138 \\ -0.5463 & -0.3051 & -0.5194 & -0.2490 & -0.5261 & -0.0000 \\ 0.2366 & 0.3102 & -0.3981 & -0.1319 & 0.0298 & -0.8192 \\ -0.4715 & -0.4706 & 0.4171 & 0.1477 & 0.2807 & -0.5307 \end{bmatrix} \tag{86}$$

The SVD's also provide 5 non-zero singular values and hence $r_C|_1 = r_C|_2 = 5$. This result confirms that there is a single inextensional mechanism in each configuration. Therefore, the inextensional mechanisms are provided by the last columns of $\mathbf{W}|_1$ and $\mathbf{W}|_2$:

$$\mathbf{W}_m|_1 = \begin{bmatrix} -0.8023 \\ -0.1415 \\ 0.5379 \\ 0.0000 \\ -0.0401 \\ 0.2130 \end{bmatrix} \quad \text{and} \quad \mathbf{W}_m|_2 = \begin{bmatrix} -0.0401 \\ -0.0071 \\ -0.2138 \\ -0.0000 \\ -0.8192 \\ -0.5307 \end{bmatrix}. \tag{87}$$

The next step is finding the second-order extensions of the skeleton structure (there are no second-order rotations because in this example there are no rigid hinges) associated with each mechanism, using Eq. (52). The matrices involved in the calculation are shown in the Appendix and the outcome of this calculation is:

$$\mathbf{e}_1 = \begin{bmatrix} 0.4765 \\ 0.0235 \\ 0.3707 \\ 0.2954 \\ 0.0153 \end{bmatrix} (\alpha^1)^2 \quad \text{and} \quad \mathbf{e}_2 = \begin{bmatrix} 0.0237 \\ 0.4763 \\ 0.0184 \\ 0.2962 \\ 0.3109 \end{bmatrix} (\alpha^2)^2 \tag{88}$$

The correcting displacements are then obtained from Eq. (58), where:

$$\mathbf{W}_c|_i = -\mathbf{W}_{r_c}|_i (\mathbf{V}_{r_c})_i^{-1} (\mathbf{U}_{r_c})_i^{\mathrm{T}} \mathbf{e}_i \tag{89}$$

with

$$\mathbf{U}_{r_c}|_1 = \begin{bmatrix} 0.3160 & -0.6138 & 0.1315 & 0.4655 & -0.5380 \\ 0.4354 & 0.3742 & 0.3573 & -0.5137 & -0.5281 \\ 0.0441 & -0.5644 & 0.5538 & -0.4320 & 0.4314 \\ 0.7864 & -0.0808 & -0.4928 & -0.0957 & 0.3507 \\ 0.3003 & 0.3978 & 0.5526 & 0.5690 & 0.3499 \end{bmatrix}, \tag{90}$$

$$\mathbf{U}_{rc}|_2 = \begin{bmatrix} 0.2824 & -0.5328 & -0.5090 & 0.6041 & 0.1110 \\ 0.3326 & 0.4670 & -0.6854 & -0.2530 & -0.3708 \\ 0.3044 & -0.5355 & -0.0878 & -0.7371 & 0.2637 \\ 0.7402 & -0.0406 & 0.5109 & 0.1251 & -0.4168 \\ 0.4111 & 0.4578 & 0.0494 & 0.1100 & 0.7790 \end{bmatrix}, \tag{91}$$

$$(\mathbf{V}_{rc})_1^{-1} = \begin{bmatrix} 0.6098 & 0 & 0 & 0 & 0 \\ 0 & 0.7725 & 0 & 0 & 0 \\ 0 & 0 & 0.8777 & 0 & 0 \\ 0 & 0 & 0 & 1.9201 & 0 \\ 0 & 0 & 0 & 0 & 3.9063 \end{bmatrix}, \tag{92}$$

and

$$(\mathbf{V}_{rc})_2^{-1} = \begin{bmatrix} 0.5442 & 0 & 0 & 0 & 0 \\ 0 & 0.7681 & 0 & 0 & 0 \\ 0 & 0 & 1.4654 & 0 & 0 \\ 0 & 0 & 0 & 1.6932 & 0 \\ 0 & 0 & 0 & 0 & 2.9735 \end{bmatrix}. \tag{93}$$

$\mathbf{W}_{rc}|_1$ and $\mathbf{W}_{rc}|_2$ are given in Eqs. (85) and (86).

The results of this calculation are:

$$\mathbf{W}_c|_1 = \begin{bmatrix} 0.2529 \\ 0.0446 \\ 0.4103 \\ -0.0000 \\ 0.0332 \\ -0.0476 \end{bmatrix} (\alpha^1)^2 \quad \text{and} \quad \mathbf{W}_c|_2 = \begin{bmatrix} -0.0332 \\ -0.0058 \\ -0.0482 \\ 0.0000 \\ -0.2529 \\ 0.4124 \end{bmatrix} (\alpha^2)^2 \tag{94}$$

6.4. Matrices for equilibrium and stability constraints

The compatibility matrices for the torsional springs are needed to form the equilibrium equations in the target configurations, Eq. (76). They are:

$$\mathbf{C}^s|_1 = \begin{bmatrix} 0 & 0 & 0 & 0 & -0.1881 & 0.9978 \\ -0.8345 & -0.1472 & 0.5594 & 0 & 0 & 0 \\ 0.2898 & 0.0184 & -0.1973 & -0.8345 & 0.0410 & 0.5770 \\ -0.8345 & 0.0410 & 0.5770 & 0.1449 & -0.0398 & 0.0731 \end{bmatrix}, \tag{95}$$

and

$$\mathbf{C}^s|_2 = \begin{bmatrix} 0 & 0 & 0 & 0 & -0.8522 & -0.5521 \\ -0.1871 & -0.0330 & -0.9975 & 0 & 0 & 0 \\ 0.0650 & -0.1365 & 0.0742 & -0.1871 & 0.8192 & 0.5700 \\ -0.1871 & 0.8192 & 0.5700 & 0.0325 & -0.2902 & -0.1949 \end{bmatrix}. \tag{96}$$

The second-order compatibility matrices for the torsional springs are needed to evaluate Eq. (77). From Eq. (68), they can be written and calculated as follows:

$$\mathbf{B}^s|_1 = \mathbf{C}^s|_1 \mathbf{W}_c|_1 + \frac{1}{2} \begin{bmatrix} \vdots \\ (\mathbf{W}_m|_1)_r^{\mathrm{T}} \mathbf{H}_r^{ts}|_1 (\mathbf{W}_m|_1)_r \\ \vdots \end{bmatrix} = \begin{bmatrix} -0.0538 \\ 0.0119 \\ -0.0330 \\ 0.0227 \end{bmatrix} + \begin{bmatrix} -0.0000 \\ 0 \\ 0.0868 \\ -0.0108 \end{bmatrix} = \begin{bmatrix} -0.0538 \\ 0.0119 \\ 0.0538 \\ 0.0119 \end{bmatrix} \tag{97}$$

and

$$\mathbf{B}^s|_2 = \mathbf{C}^s|_2 \mathbf{W}_c|_2 + \frac{1}{2} \begin{bmatrix} \vdots \\ (\mathbf{W}_m|_2)_r^{\mathrm{T}} \mathbf{H}_r^{ts}|_2 (\mathbf{W}_m|_2)_r \\ \vdots \end{bmatrix} = \begin{bmatrix} -0.0122 \\ 0.0545 \\ 0.0230 \\ -0.0330 \end{bmatrix} + \begin{bmatrix} 0.0000 \\ -0.0000 \\ -0.0108 \\ 0.0876 \end{bmatrix} = \begin{bmatrix} -0.0122 \\ 0.0545 \\ 0.0122 \\ 0.0545 \end{bmatrix} \tag{98}$$

Details on the calculation of $(\mathbf{W}_m|_i)_r^{\mathrm{T}} \mathbf{H}_r^{ts}|_i (\mathbf{W}_m|_i)_r$ for the four torsional springs are provided in the Appendix.
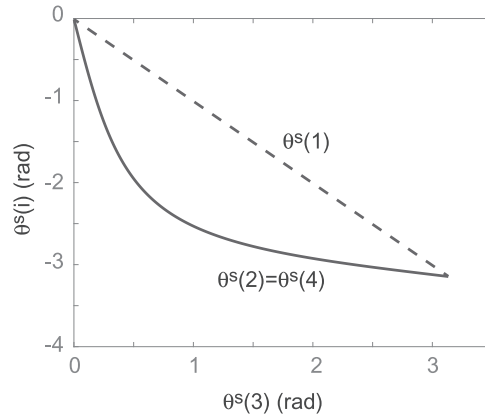
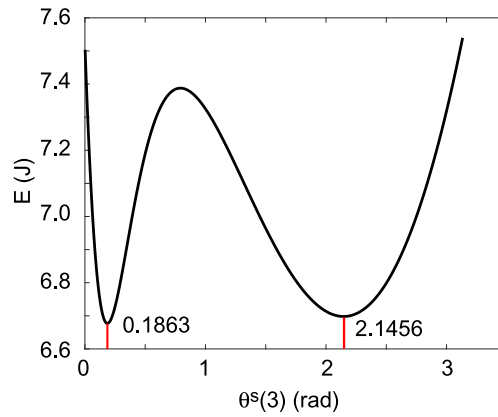**Fig. 9.** Variation of hinge rotations.

Fig. 10. Strain energy variation and values of $\theta^s(3)$ for which the energy has a local minimum.

6.5. Equilibrium and stability conditions

Substituting Eqs. (87), (95) and (96) into (76) gives the equilibrium equations in the two target configurations. Then, moving all known quantities to the right hand side of Eq. (76) gives:

$$\begin{bmatrix} 0.2201 & 0.9913 & -0.2201 & 0.9913 \\ 0.9911 & 0.2210 & -0.9911 & 0.2210 \end{bmatrix} \boldsymbol{\theta}_0^s = \begin{bmatrix} 2.0394 \\ 5.5584 \end{bmatrix} \tag{99}$$

The stability conditions are obtained by substituting Eqs. (87), (95), (96), (A.13) and (98) with $\mathbf{K} = \mathbf{I}$ into Eq. (77). Then, moving all known quantities to the right hand side of the inequality gives:

$$\begin{bmatrix} -0.0538 & 0.0119 & 0.0538 & 0.0119 \\ -0.0122 & 0.0545 & 0.0122 & 0.0545 \end{bmatrix} \boldsymbol{\theta}_0^s > \begin{bmatrix} -1.0276 \\ -0.7612 \end{bmatrix} \tag{100}$$

A unique design solution of Eqs. (99)–(100) can be obtained by choosing to minimize $|\boldsymbol{\theta}_0^s|^2$ and solving a quadratic programming problem, which has been done with the function quadprog in Matlab:

$$\boldsymbol{\theta}_0^s = \begin{bmatrix} 2.7089 \\ 0.4273 \\ -2.7089 \\ 0.4273 \end{bmatrix} \text{rad} = \begin{bmatrix} 155.2095° \\ 24.4834° \\ -155.2095° \\ 24.4834° \end{bmatrix} \tag{101}$$

The rest angles of the springs are $-\boldsymbol{\theta}_0^s$. Note that different designs can be obtained if one does not choose to minimize the norm of the initial spring rotations.

The variation of the hinge rotations for the range $\theta^s(3) = (0, \pi)$ rad has been computed using the algorithm in Kumar and Pellegrino (2000) and has been plotted in Fig. 9. Assigning the spring stiffness as 1 N·m/rad, the corresponding variation of the strain energy variation is shown in Fig. 10. It shows that both target configurations correspond to a local minimum.
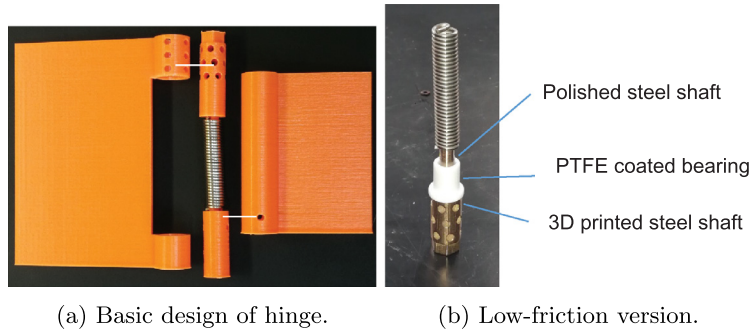
(a) Basic design of hinge.   (b) Low-friction version.

Fig. 11. Hinge design with adjustable angle.

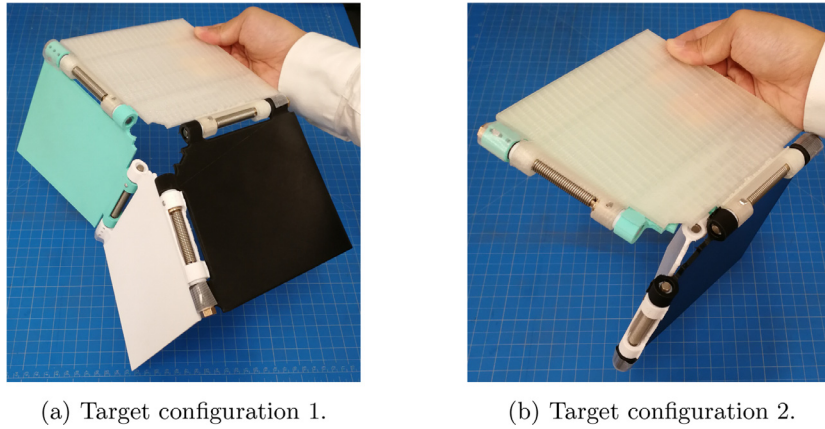(a) Target configuration 1.   (b) Target configuration 2.

Fig. 12. Two stable configurations of the prototype.

6.6. Proof of concept model

An important aspect of building physical models of the structures described in this paper is the construction of hinges with the required initial angles. A simple design concept was borrowed from post-stressed door spring hinges (Global, 2018), shown in Fig. 11. In Fig. 11a, two shafts are connected by a torsional spring; the top shaft is connected to the left plate while the bottom is connected to the right plate. The initial angle of the hinge can be set to an accuracy of $10°$. A low-friction version, with a thinner and polished shaft with a PTFE coated bearing is shown in Fig. 11b.

A plastic model was printed with a CraftUnique CraftBot Plus 3D printer. The steel torsional springs were TO-1027 from Century Spring Corp. and the PTFE bearings were model 2706T14 from McMaster-Carr. Based on the design in Eq. (101), the initial spring rotations were set to $\boldsymbol{\theta}_0^s = \begin{bmatrix} 160° & 20° & -160° & 20° \end{bmatrix}^{\mathrm{T}}$. The assembled structure is shown in Fig. 12 held by its top-right panel. The existence of the two target stable configurations was verified with the model.

7. Conclusion

This paper has presented a new, general formulation for the design of morphing bar and plate structures which are rendered multi-stable in a set of chosen target configurations, through extensional and rotational linear-elastic springs whose stiffness and initial length/angle are specifically chosen to achieve this desired behavior.

The design process starts with a skeleton structure, i.e. a mechanism consisting of rigid bars and plates that can achieve the required target configurations through a continuous kinematic deformation. It is emphasized that the synthesis of skeleton structures with practically useful target configurations that are also connected by a continuous kinematic manifold is a separate and challenging problem in itself. An example of achieving desired shapes for a specific three-dimensional skeleton structure can be found in Liao and McCarthy (2001). Currently, there are no general methods to carry out this task.

At the beginning of the analysis, a reference configuration of the structure as well as the chosen target configurations are defined. The compatibility matrix of the structure and its singular value decomposition are computed in each target configuration, and from these decompositions the rank of the compatibility matrix and a set of independent zero-energy mechanisms are computed for each target configuration. Then, the second-order extensions of the bars and the rotations of the hinges that are associated with unit amplitudes of the independent mechanisms are computed using Eq. (52). The second-order nodal displacements that correct these extensions/rotations are computed using Eqs. (58), (59) and (61). This

calculation yields the independent second-order zero-energy mechanisms of the skeleton structure, according to Eq. (62). Then, extensional and torsional springs are introduced in the structure and the compatibility and Hessian matrices for these springs are computed. With these matrices, the second-order extensions and rotations of the springs are computed for each independent mechanism of the skeleton structure, using Eqs. (66)–(68). Lastly, a set of equilibrium equations and stability inequalities are computed for each target configuration, using Eqs. (76)–(77).

This final step completes the formulation of the design problem, whose solution —consisting of the stiffness and initial length/angle of each spring— is in general not unique. At this point a cost function can be introduced and the minimization of this function, subject to the constraint equations, is a constrained optimization problem that can be solved numerically. A key advantage of the developed method is its full generality.

Follow-on research suggested by the present research includes the explicit trade-off between the number and position of extensional and rotational springs. Are the two types of springs equivalent in terms of the features of energy surface that can be created? Also, in some specific applications it may be desirable that the local energy minima are separated by a high energy maximum, to prevent accidental triggering of a shape change. What determines the highest energy barrier that can be achieved? Lastly, a theory to design multi-stable morphing structures using nonlinear springs would be an obvious next step.

Another open research topic is the development of efficient manufacturing techniques to build structures with the required spring properties, as the approach used for the proof-concept model in Section 6 would not be suitable for larger structures.

Research Data

Matlab codes for the example in Section 6 can be downloaded from Supplementary material. Download all files and put them in the same folder. Run the script ''RUN_ME_miura_phi0'' in Matlab and the design parameters (rest angles for the torsional springs) will be computed.

Declaration of Competing Interest

None.

Acknowledgments

Appendix A

This appendix provides further details on the results presented in Section 6. The matrices $\mathbf{A}_k^b$ to calculate Eq. (52) for the two target configurations are computed from Eq. (38) with $\widetilde{\mathbf{H}}$ defined in Eq. (17). Note that the compatibility matrices of bars 1, 2 and 5 are not calculated because both end nodes are constrained.

For the first configuration:

$$\mathbf{A}_3^b|_1 = \frac{1}{2 \times 1}\begin{bmatrix} -0.8023 \\ -0.1415 \\ 0.5379 \end{bmatrix}^{\mathrm{T}} \widetilde{\mathbf{H}} \begin{bmatrix} -0.8023 \\ -0.1415 \\ 0.5379 \end{bmatrix} = 0.4765 \tag{A.1}$$

$$\mathbf{A}_4^b|_1 = \frac{1}{2 \times 1}\begin{bmatrix} 0.0000 \\ -0.0401 \\ 0.2130 \end{bmatrix}^{\mathrm{T}} \widetilde{\mathbf{H}} \begin{bmatrix} 0.0000 \\ -0.0401 \\ 0.2130 \end{bmatrix} = 0.0235 \tag{A.2}$$

$$\mathbf{A}_6^b|_1 = \frac{1}{2 \times 1.2856}\begin{bmatrix} -0.8023 \\ -0.1415 \\ 0.5379 \end{bmatrix}^{\mathrm{T}} \widetilde{\mathbf{H}} \begin{bmatrix} -0.8023 \\ -0.1415 \\ 0.5379 \end{bmatrix} = 0.3707 \tag{A.3}$$

$$\mathbf{A}_7^b|_1 = \frac{1}{2 \times 1.2856}\begin{bmatrix} -0.8023 \\ -0.1415 \\ 0.5379 \\ 0.0000 \\ -0.0401 \\ 0.2130 \end{bmatrix}^{\mathrm{T}} \widetilde{\mathbf{H}} \begin{bmatrix} -0.8023 \\ -0.1415 \\ 0.5379 \\ 0.0000 \\ -0.0401 \\ 0.2130 \end{bmatrix} = 0.2954 \tag{A.4}$$

$$\mathbf{A}_8^b|_1 = \frac{1}{2 \times 1.5321} \begin{bmatrix} 0.0000 \\ -0.0401 \\ 0.2130 \end{bmatrix}^{\mathrm{T}} \widetilde{\mathbf{H}} \begin{bmatrix} 0.0000 \\ -0.0401 \\ 0.2130 \end{bmatrix} = 0.0153 \tag{A.5}$$

For the second configuration:

$$\mathbf{A}_3^b|_2 = \frac{1}{2 \times 1} \begin{bmatrix} -0.0401 \\ -0.0071 \\ -0.2138 \end{bmatrix}^{\mathrm{T}} \widetilde{\mathbf{H}} \begin{bmatrix} -0.0401 \\ -0.0071 \\ -0.2138 \end{bmatrix} = 0.0237 \tag{A.6}$$

$$\mathbf{A}_4^b|_2 = \frac{1}{2 \times 1} \begin{bmatrix} -0.0000 \\ -0.8192 \\ -0.5307 \end{bmatrix}^{\mathrm{T}} \widetilde{\mathbf{H}} \begin{bmatrix} -0.0000 \\ -0.8192 \\ -0.5307 \end{bmatrix} = 0.4763 \tag{A.7}$$

$$\mathbf{A}_6^b|_2 = \frac{1}{2 \times 1.2856} \begin{bmatrix} -0.0401 \\ -0.0071 \\ -0.2138 \end{bmatrix}^{\mathrm{T}} \widetilde{\mathbf{H}} \begin{bmatrix} -0.0401 \\ -0.0071 \\ -0.2138 \end{bmatrix} = 0.0184 \tag{A.8}$$

$$\mathbf{A}_7^b|_2 = \frac{1}{2 \times 1.2856} \begin{bmatrix} -0.0401 \\ -0.0071 \\ -0.2138 \\ -0.0000 \\ -0.8192 \\ -0.5307 \end{bmatrix}^{\mathrm{T}} \widetilde{\mathbf{H}} \begin{bmatrix} -0.0401 \\ -0.0071 \\ -0.2138 \\ -0.0000 \\ -0.8192 \\ -0.5307 \end{bmatrix} = 0.2962 \tag{A.9}$$

$$\mathbf{A}_8^b|_2 = \frac{1}{2 \times 1.5321} \begin{bmatrix} -0.0000 \\ -0.8192 \\ -0.5307 \end{bmatrix}^{\mathrm{T}} \widetilde{\mathbf{H}} \begin{bmatrix} -0.0000 \\ -0.8192 \\ -0.5307 \end{bmatrix} = 0.3109 \tag{A.10}$$

The calculation of the second-order compatibility matrices for the torsional springs involves a separate calculation for each spring. The Hessian matrices for the rotational springs are obtained from Eqs. A(10) to A(20) in Appendix A of Liu and Paulino (2017). Nodes pinned to the ground are not included in the calculation.

For the first configuration:

spring 1: $(1/2)(\mathbf{W}_m|_1)_1^{\mathrm{T}} \mathbf{H}_1^{ts}|_1 (\mathbf{W}_m|_1)_1 =$

$$= \frac{1}{2} \begin{bmatrix} 0.0000 \\ -0.0401 \\ 0.2130 \end{bmatrix}^{\mathrm{T}} \begin{bmatrix} 0 & 0 & 0 \\ 0 & -0.3754 & 0.9603 \\ 0 & 0.9603 & 0.3754 \end{bmatrix} \begin{bmatrix} 0.0000 \\ -0.0401 \\ 0.2130 \end{bmatrix} = 0 \tag{A.11}$$

spring 2: $(1/2)(\mathbf{W}_m|_1)_2^{\mathrm{T}} \mathbf{H}_2^{ts}|_1 (\mathbf{W}_m|_1)_2 =$

$$= \frac{1}{2} \begin{bmatrix} -0.8023 \\ -0.1415 \\ 0.5379 \end{bmatrix}^{\mathrm{T}} \begin{bmatrix} -0.9196 & -0.1621 & -0.3990 \\ -0.1621 & -0.0286 & -0.0704 \\ -0.3990 & -0.0704 & 0.9482 \end{bmatrix} \begin{bmatrix} -0.8023 \\ -0.1415 \\ 0.5379 \end{bmatrix} = 0 \tag{A.12}$$

spring 3: $(1/2)(\mathbf{W}_m|_1)_3^{\mathrm{T}} \mathbf{H}_3^{ts}|_1 (\mathbf{W}_m|_1)_3 =$

$$= \frac{1}{2} \begin{bmatrix} -0.8023 \\ -0.1415 \\ 0.5379 \\ 0.0000 \\ -0.0401 \\ 0.2130 \end{bmatrix}^{\mathrm{T}} \begin{bmatrix} 0.1931 & -0.0204 & 0.2181 & -0.4485 & 0.2101 & -0.6878 \\ -0.0204 & 0.1917 & 0.0543 & 0.1692 & -0.0175 & -0.0680 \\ 0.2181 & 0.0543 & -0.3848 & 0.3238 & -0.1460 & 0.4660 \\ -0.4485 & 0.1692 & 0.3238 & -0.1302 & -0.8410 & 0.0108 \\ 0.2101 & -0.0175 & -0.1460 & -0.8410 & 0.0829 & 0.5854 \\ -0.6878 & -0.0680 & 0.4660 & 0.0108 & 0.5854 & 0.0473 \end{bmatrix} \begin{bmatrix} -0.8023 \\ -0.1415 \\ 0.5379 \\ 0.0000 \\ -0.0401 \\ 0.2130 \end{bmatrix}$$
$$= 0.0868 \tag{A.13}$$

spring 4: $(1/2)(\mathbf{W}_m|_1)_4^{\mathrm{T}} \mathbf{H}_4^{ts}|_1 (\mathbf{W}_m|_1)_4 =$

$$= \frac{1}{2} \begin{bmatrix} -0.8023 \\ -0.1415 \\ 0.5379 \\ 0.0000 \\ -0.0401 \\ 0.2130 \end{bmatrix}^{\mathrm{T}} \begin{bmatrix} -0.9196 & 0.2333 & -0.3620 & 0.0148 & -0.0334 & 0.1631 \\ 0.2333 & -0.0207 & -0.1123 & -0.8481 & 0.0432 & 0.5779 \\ -0.3620 & -0.1123 & 0.9403 & -0.0894 & 0.0270 & -0.0580 \\ 0.0148 & -0.8481 & -0.0894 & -0.4233 & 0.3504 & -0.6613 \\ -0.0334 & 0.0432 & 0.0270 & 0.3504 & -0.1212 & 0.0915 \\ 0.1631 & 0.5779 & -0.0580 & -0.6613 & 0.0915 & 0.5445 \end{bmatrix} \begin{bmatrix} -0.8023 \\ -0.1415 \\ 0.5379 \\ 0.0000 \\ -0.0401 \\ 0.2130 \end{bmatrix}$$
$$= -0.0108 \tag{A.14}$$

And for the second configuration:

spring 1: $(1/2)(\mathbf{W}_m|_2)_1^{\mathrm{T}}\mathbf{H}_1^{ts}|_2(\mathbf{W}_m|_2)_1 =$

$$= \frac{1}{2}\begin{bmatrix} 0.0000 \\ -0.0401 \\ 0.2130 \end{bmatrix}^{\mathrm{T}} \begin{bmatrix} 0 & 0 & 0 \\ 0 & 0.9410 & -0.4215 \\ 0 & -0.4215 & -0.9410 \end{bmatrix} \begin{bmatrix} 0.0000 \\ -0.0401 \\ 0.2130 \end{bmatrix} = 0 \tag{A.15}$$

spring 2: $(1/2)(\mathbf{W}_m|_2)_2^{\mathrm{T}}\mathbf{H}_2^{ts}|_2(\mathbf{W}_m|_2)_2 =$

$$= \frac{1}{2}\begin{bmatrix} -0.8023 \\ -0.1415 \\ 0.5379 \end{bmatrix}^{\mathrm{T}} \begin{bmatrix} 0.3677 & 0.0648 & 0.9443 \\ 0.0648 & 0.0114 & 0.1665 \\ 0.9443 & 0.1665 & -0.3791 \end{bmatrix} \begin{bmatrix} -0.8023 \\ -0.1415 \\ 0.5379 \end{bmatrix} = 0 \tag{A.16}$$

spring 3: $(1/2)(\mathbf{W}_m|_2)_3^{\mathrm{T}}\mathbf{H}_3^{ts}|_2(\mathbf{W}_m|_2)_3 =$

$$= \frac{1}{2}\begin{bmatrix} -0.8023 \\ -0.1415 \\ 0.5379 \\ 0.0000 \\ -0.0401 \\ 0.2130 \end{bmatrix}^{\mathrm{T}} \begin{bmatrix} -0.2527 & 0.3827 & -0.2081 & 0.1950 & -0.0015 & -0.0419 \\ 0.3827 & -0.2897 & 0.6422 & -0.8207 & -0.1379 & 0.0831 \\ -0.2081 & 0.6422 & 0.5423 & -0.5333 & -0.2611 & -0.0571 \\ 0.1950 & -0.8207 & -0.5333 & -0.1288 & 0.3740 & 0.0429 \\ -0.0015 & -0.1379 & -0.2611 & 0.3740 & -0.8051 & 0.3910 \\ -0.0419 & 0.0831 & -0.0571 & 0.0429 & 0.3910 & 0.9340 \end{bmatrix} \begin{bmatrix} -0.8023 \\ -0.1415 \\ 0.5379 \\ 0.0000 \\ -0.0401 \\ 0.2130 \end{bmatrix}$$

$$= -0.0108 \tag{A.17}$$

spring 4: $(1/2)(\mathbf{W}_m|_2)_4^{\mathrm{T}}\mathbf{H}_4^{ts}|_2(\mathbf{W}_m|_2)_4 =$

$$= \frac{1}{2}\begin{bmatrix} -0.8023 \\ -0.1415 \\ 0.5379 \\ 0.0000 \\ -0.0401 \\ 0.2130 \end{bmatrix}^{\mathrm{T}} \begin{bmatrix} 0.3677 & -0.7573 & -0.5678 & -0.0963 & 0.2738 & 0.1976 \\ -0.7573 & -0.4156 & -0.1102 & 0.2317 & -0.3665 & -0.2861 \\ -0.5678 & -0.1102 & 0.0479 & -0.0561 & 0.6962 & 0.4628 \\ -0.0963 & 0.2317 & -0.0561 & 0.2007 & -0.0189 & -0.0151 \\ 0.2738 & -0.3665 & 0.6962 & -0.0189 & 0.1809 & -0.2300 \\ 0.1976 & -0.2861 & 0.4628 & -0.0151 & -0.2300 & -0.3816 \end{bmatrix} \begin{bmatrix} -0.8023 \\ -0.1415 \\ 0.5379 \\ 0.0000 \\ -0.0401 \\ 0.2130 \end{bmatrix}$$

$$= 0.0876 \tag{A.18}$$

The complete matrices are therefore:

$$\begin{bmatrix} -0.0000 \\ 0 \\ 0.0868 \\ -0.0108 \end{bmatrix} \quad \text{and} \quad \begin{bmatrix} 0.0000 \\ -0.0000 \\ -0.0108 \\ 0.0876 \end{bmatrix} \tag{A.19}$$

Supplementary material

Supplementary material associated with this article can be found, in the online version, at doi 10.1016/j.jmps.2019.103772.

References

Arrieta, A.F., Bilgen, O., Friswell, M.I., Ermanni, P., 2013. Modelling and configuration control of wing-shaped bi-stable piezoelectric composites under aerodynamic loads. Aerosp. Sci. Technol. 29 (1), 453–461. 2013 doi: 10.1016/j.ast.2013.05.004.

Chen, G.-S., Wada, B.K., 1993. Adaptive truss manipulator space crane concept. J. Spacecraft Rockets 30, 111–115. doi:10.2514/3.25477?journalCode=jsr.

Clarricoats, P.J.B., Zhou, H., 1991. Design and performance of a reconfigurable mesh reflector antenna. 1. antenna design. IEE Proc. H - Microwaves Antennas Propag. 138 (6), 485–492. Dec 1991

Daynes, S., Nall, S.J., Weaver, P., Potter, K., Margaris, P., Mellor, P., 2010. Bistable composite flap for an airfoil. J. Aircr. 47, 334–338. https://arc.aiaa.org/doi/pdf/10.2514/1.45389?casa_token=ksWnQxnxMrwAAAAA:HE-V7X21mzzZd5xquw78yEvrqTD1HejyURlmfQsRrICvW2ajw7fm4N6qIQD86ZrpDpN2BK6SDt8r

Daynes, S., Weaver, P.M., Trevarthen, J.A., 2011. A morphing composite air inlet with multiple stable shapes. J. Intell. Mater. Syst.Struct. 22 (9), 961–973. https://journals.sagepub.com/doi/abs/10.1177/1045389X11399943

Global, 2018. Global cps3535-r-us4-m commercial grade, full mortise spring hinge. https://www.amazon.com/Global-CPS3535-R-US4-M-Commercial-Mortise-Spring/dp/B00164JZOQ.

Jensen, B.D., Howell, L.L., 2004. Identification of compliant pseudo-rigid-body four link mechanism configurations resulting in bistable behavior. ASME J. Mech. Des. 125 (4), 701–708. doi:10.1115/1.1625399.

Jensen, B.D., Howell, L.L., Salmon, L.G., 1999. Design of two-link, in-plane, bistable compliant micro-mechanisms. ASME J. Mech. Des. 121 (3), 416–423. doi:10.1115/1.2829477.

King, C., Campbell, M., Beaman, J., Sreenivasan, S., 2005. Synthesis of multistable equilibrium linkage systems using an optimization approach. Struct. Multidiscip. Optim. 29 (6), 477–487. doi:10.1007/s00158-004-0489-6.

Kumar, P., Pellegrino, S., 2000. Computation of kinematic paths and bifurcation points. Int. J. Solids Struct. 37 (46), 7003–7027. doi:10.1016/S0020-7683(99)00327-3.

Li, Y., Pellegrino, S., 2018. Design of structures with multiple equilibrium configurations. In: ASME. IDETC-CIE Volume 5B: 42nd Mechanisms and Robotics Conference doi:10.1115/DETC2018-86157.

Liao, Q., McCarthy, J.M., 2001. On the seven position synthesis of a 5-SS platform linkage. J. Mech. Des. 123 (1), 74–79.

Liu, K., Paulino, G.H., 2017. Nonlinear mechanics of non-rigid origami: an efficient computational approach. Proc. R. Soc. London A 473 (2206). doi:10.1098/rspa.2017.0348.

Matlab, 2018. Mathworks, 1 apple hill drive, natick, MA.

Mc Carthy, J.M., Soh, G.S., 2010. Geometric Design of Linkages (Vol. 11). Springer Science & Business Media.

Miura, K., 1970. Proposition of pseudo-cylindrical concave polyhedral shells. IASS Symposium on Folded Plates and Prismatic Structures, Vienna.

Miura, K., Furuya, H., Suzuki, K., 1985. Variable geometry truss and its application to deployable truss and space crane arm. Acta Astronautica 12, 599–607.

Niu, C., 2011. Airframe Stress Analysis and Sizing, Second edition Conmilit Press.

Pellegrino, S., 1993. Structural computations with the singular value decomposition of the equilibrium matrix. Int. J. Solids Struct. 30 (21), 3025–3035. doi:10.1016/0020-7683(93)90210-X.

Pellegrino, S., Calladine, C.R., 1986. Matrix analysis of statically and kinematically indeterminate frameworks. Int. J. Solids Struct. 22 (4), 409–428. https://www.sciencedirect.com/science/article/pii/0020768386900144

Rhodes, M.D., Mikulas, M.M., 1985. Deployable controllable geometry truss beam. NASA langley research center. Report NASA TM-86366.

Schenk, M., Guest, S.D., 2013. Geometry of miura-folded metamaterials. PNAS 110, 3276–3281.

Schioler, T., Pellegrino, S., 2007. Space frames with multiple stable configurations. AIAA J. 45, 1740–1747. https://arc.aiaa.org/doi/pdf/10.2514/1.16825?casa_token=gUx2YkDMc1MAAAAA:CUiwaz_yNk4xyrAAVh-argUYrkL7ETXrECm5PZh8iICsDtmJhwZqcAlROIsDVJO_YiIZ41JnBh4n.

Stern, M., Pinson, M. B., Murugan, A., 2019. Learned multi-stability in mechanical networks. http://arxiv.org/abs/arXiv:1902.08317.

Strang, G., 2006. Linear algebra and its applications. Thomson, Brooks/Cole. https://books.google.com/books?id=8QVdcRJyL2oC.

Su, H.J., Mc Carthy, J.M., 2007. Synthesis of bistable compliant four-bar mechanisms using polynomial homotopy. J. Mech. Des. 129 (10), 1094–1098. http://mechanicaldesign.asmedigitalcollection.asme.org/article.aspx?articleid=1449539.

Thompson, J.M.T., Hunt, G.W., 1984. Elastic Instability Phenomena. Wiley-Interscience, New York.

Venkiteswaran, V.K., Su, H.J., 2018. A versatile 3r pseudo-rigid-body model for initially curved and straight compliant beams of uniform cross section. J. Mech. Des. 140 (5), 092305. September 2018.

Wada, B.K., Fanson, J.L., Crawley, E.F., 1990. Adaptive structures. J. Intell. Mater. Syst.Struct. 1 (2), 157–174.

Wagg, D., Bond, I., Weaver, P., Friswell, M., 2008. Adaptive Structures: Engineering Applications. John Wiley & Sons.

Waitukaitis, S., Menaut, R., Chen, B.G.-g., van Hecke, M., 2015. Origami multistability: from single vertices to metasheets. Phys. Rev. Lett. 114 (2015), 055503. doi:10.1103/PhysRevLett.114.055503.

Washington, G., 1996. Smart aperture antennas. Smart Mater. Struct. 5 (6), 801. http://stacks.iop.org/0964-1726/5/i=6/a=010.